EX SITU STUDY OF THE EPITAXIAL GROWTH OF *N*-ALKANE THIN FILMS

A Thesis Submitted to the College of

Graduate Studies and Research

In Partial Fulfillment of the Requirements

For the Degree of Master of Science

In the Department of Chemistry

University of Saskatchewan

Saskatoon

By

CURTIS SENGER

PERMISSION TO USE

In presenting this thesis/dissertation in partial fulfillment of the requirements for a Postgraduate degree from the University of Saskatchewan, I agree that the Libraries of this University may make it freely available for inspection. I further agree that permission for copying of this thesis/dissertation in any manner, in whole or in part, for scholarly purposes may be granted by the professor or professors who supervised my thesis/dissertation work or, in their absence, by the Head of the Department or the Dean of the College in which my thesis work was done. It is understood that any copying or publication or use of this thesis/dissertation or parts thereof for financial gain shall not be allowed without my written permission. It is also understood that due recognition shall be given to me and to the University of Saskatchewan in any scholarly use which may be made of any material in my thesis/dissertation.

Requests for permission to copy or to make other uses of materials in this thesis/dissertation in whole or part should be addressed to:

Head of the Department of Chemistry

110 Science Place

University of Saskatchewan

Saskatoon, Saskatchewan S7N 5C9

Canada

Abstract

A thorough understanding of the growth mechanism in organic thin film growth is necessary to be able to develop devices based on these materials. In particular, there are open questions about the growth mechanism of multilayered structures beyond the first monolayer. Of particular interest to this work is developing an understanding of the early and intermediate steps of *n*-alkane film epitaxial growth on highly ordered surfaces.

In order to address this question, a technique needs to be used that allows observation of films at intervals during growth, while providing elemental sensitivity, spatial resolution, and orientation information. Photoemission electron microscopy (PEEM) is an electron microscopy technique with high spatial resolution suited to studying thin films *in situ*. When combined with tunable polarized X-rays from a synchrotron source, PEEM provides a powerful method to study the orientation of molecular films.

However, alkane films are sensitive to radiation damage from UV and X-ray light. In addition, an *in situ* deposition study of *n*-alkanes cannot be performed without contamination of the vacuum environment. Deposition in PEEM will lead to contamination of other samples when the microscope is subsequently used. Therefore, an *ex situ* approach is used, where films are grown in high vacuum conditions in an adjacent chamber and analyzed with PEEM immediately after preparation. This method will be used to study the intermediate stages of *n*-alkane thin film growth.

Previous research using linear polarized near edge X-ray absorption spectroscopy (NEXAFS) has proven useful in the study of the various oriented morphologies of *n*-alkanes grown by physical vapour deposition. Early to mid-stage growth has not been studied in depth however, and there may be a shift in growth modes as the epitaxial interaction with the graphite substrate is reduced as more layers are deposited. The *ex situ* evaporator has been designed, manufactured, and is operating according to expectations. Experiments have been performed to address the compatibility of these alkanes in the PEEM with x-ray illumination, including normalization techniques and radiation damage assessment.

Acknowledgements

I would like to express my utmost gratitude to my supervisor, Professor Stephen Urquhart. He has always been there to guide me towards the next step of the research process, and to patiently point me in the right direction when things are not going as planned. I would also like to thank the members of my advisory committee, Professors Richard Bowles and Matthew Paige, who have helped to guide me through these past few years. I would also like to give a special thanks to the staff of the Canadian Light Source, particularly Dr. Jian Wang for his invaluable training and support for the PEEM.

I am sincerely grateful for the help of the staff of the Physics Machine Shop, Ted Toporowski, Blair Chomyshen, and Jill Cornish. Without their combined experience and expertise, my far-fetched designs would never have become a reality. I would also like to extend my gratitude to Leah Hildebrandt for her help and support.

I wish to give my thanks to my groupmates Sahan Perera, Sadegh Shokatian, and Amara Zuhaib for their support and help with experiment planning, data interpretation, and writing advice. Finally, I would like to express my gratitude to my friends and family. Their encouragement and faith in me are what has made this project a reality.

Table of Contents

List of Figures

List of Acronyms and Symbols

AFM	Atomic Force Microscopy
C36	n-$C_{36}H_{74}$, Hexatriacontane
CaPeRS	Canadian Photoelectron Research Spectromicroscope
CCD	Charge Coupled Device
$\vec{E}$	Electric Field Vector
HOPG	Highly Oriented Pyrolytic Graphite
MCP	Multi-Channel Plate
NEXAFS	Near Edge X-ray Absorption Fine Structure
PEEM	Photoemission Electron Microscope
PVD	Physical Vapour Deposition
RTD	Resistance Temperature Detector
STXM	Scanning Transmission X-ray Microscope
SM	Spectromicroscopy
T_S	Substrate Temperature
T_{SC}	Super Cooling Temperature
TDM	Transition Dipole Moment
UHV	Ultra High Vacuum
UV	Ultraviolet
XAS	X-ray Absorption Spectroscopy

Chapter 1 - Background and Introduction

Ordering and arrangement in molecular thin films is an important subject for many areas of research, particularly for optical and organic coatings, as well as electronic devices, such as thin film semiconductors[1-3]. It is important to understand these growth phenomena in order to adjust specific properties in the final film. The growth mechanisms for monolayer organic films can be studied with precision using high resolution scanning tunneling and atomic force microscopy (AFM)[4-6], as atomic or molecular resolution is possible. Multilayer films are inherently more complex and their structures cannot necessarily be inferred from monolayer studies. For example, adsorbate-adsorbate interactions become important as layers are added, and there can be a transition from molecule-substrate to intermolecular interactions during film growth. The change to intermolecular forces causes variations in the growth mechanism, film structure, and morphology.

Linear dichroism in near edge X-ray absorption fine structure (NEXAFS) spectroscopy has been used to provide information on the molecular orientation of *n*-alkane films[7]. When combined with photoemission electron microscopy (PEEM), this technique can be used to provide information on individual areas of a film, with a spatial resolution down to 100nm. In this project, the orientation of *n*-alkane films will be studied by X-ray linear dichroism in NEXAFS spectroscopy measured by PEEM. As *n*-alkane films are easily damaged by X-ray radiation, care must be taken to minimize the effect of radiation damage on the samples. The primary goal of this project is to investigate the early to intermediate stage growth of *n*-alkane films on a highly ordered surface. To address this, an *ex situ* evaporator will be designed and manufactured. This will allow films to be prepared on site and studied immediately thereafter, without exposure to the atmosphere.

1.1 Near Edge X-ray Absorption Fine Structure Spectroscopy (NEXAFS)

NEXAFS is an element specific X-ray absorption spectroscopy (XAS) technique. A sharp rise in absorption occurs when the energy of the absorbing X-ray corresponds to the binding energy of a core electron. This abrupt discontinuity in the absorption probability is known as the absorption edge and will be described in detail below. In addition to elemental sensitivity, NEXAFS spectra of low Z elements are sensitive to chemical bonding, oxidation states, and functional groups. This means that NEXAFS can be used to gather information about the local environment of specific elements in a molecule.

NEXAFS can also be used to provide information about molecular orientation of a sample. When there exists an ordered arrangement of molecules, the intensity of the features in the NEXAFS spectrum depend on the orientation of the transition dipole moment (TDM) relative to the polarization vector of a linearly polarized X-ray beam. If the angle between the polarization vector of the illuminating X-rays and the TDM is varied, easily observed changes in the NEXAFS spectrum are produced[8]. This is termed linear dichroism and is used to determine the orientation of *n*-alkane molecules at the surface of an ordered film. The NEXAFS spectrum is therefore sensitive to molecular orientation. For these reasons NEXAFS is powerful technique for observing highly ordered domains in a molecular thin film.

1.1.1 Principles of NEXAFS Spectroscopy

XAS is the measurement of the photobsorption cross section of a substance at X-ray wavelengths. NEXAFS is a type of XAS that concerns spectra with an energy range a few eV below the absorption edge to around 50 eV above the edge[8]. X-ray absorption can excite or ionize core electrons, creating a core hole. In general, the X-ray absorption cross section of a material decreases with increasing photon energy. At discrete energies a sharp increase in absorption is observed. This abrupt discontinuity in the absorption probability is known as the absorption edge. To illustrate this effect, the theoretical absorption cross section of copper is shown in Figure 1-1. The absorption edges of copper are clearly visible as sharp increases in absorption. The energy where the absorption edge occurs is unique to individual elements and corresponds to the shell that is being excited (1s, 2s, 2p, etc.).

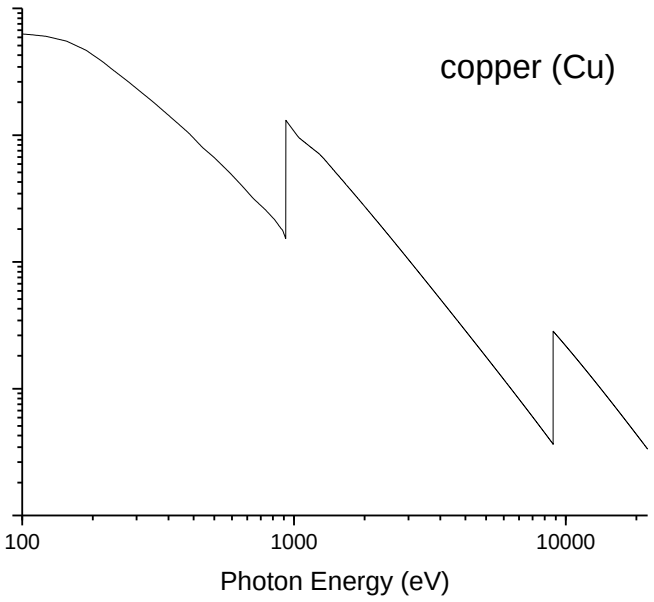

Figure 1-1: Theoretical absorption cross section for copper. Data used from Henke *et al*.[9]

X-ray absorption is followed by a decay process, as shown in Figure 1-2, below. The creation of a core hole is caused by the absorption of an X-ray causing a photoelectron to be ejected from the atom. The core excited state is short-lived and a series of relaxation processes occur to bring the atom back to the ground state. The empty core hole can be quickly filled by an electron in a higher energy orbital, leading to a fluorescent photon to be emitted with an energy characteristic of the atom. The energy of the electron decaying to fill the core hole may also be transferred to a shell electron which is then ejected from the atom, called an Auger electron. The X-ray absorption spectrum is produced by measuring the amount of emitted Auger electrons, or the amount of fluorescent photons emitted, as a function of photon energy[8].

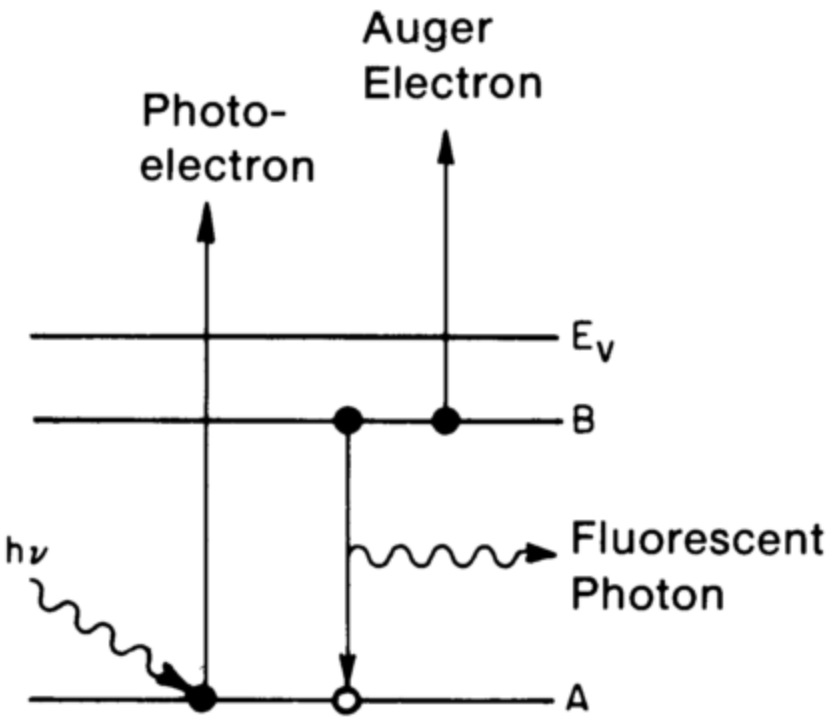

Figure 1-2: Diagram of X-ray absorption and decay processes. Energy that is charcteristic of an atom is released, either as an Auger electron or a fluorescent photon, when the cole hole is filled from an electron from a higher shell. Figure reprinted from Hahner[10] with permission.

The relative fluorescence and Auger yield is strongly related to the atomic number Z as shown in Figure 1-3. For the 1s core holes, Auger decay has a higher probability than fluorescence in low Z atoms, and therefore dominates the decay process. Similar relationships between atomic number and relative yields exist for 1s and 2p transitions[11]. Auger decay is favored for the low Z elements, such as carbon, nitrogen and oxygen. Consequently, electron yield measurement is the preferred way to obtain a NEXAFS spectrum for low Z elements. Auger electrons are not observed for helium and hydrogen, since the Auger decay process requires at least three electrons[8].

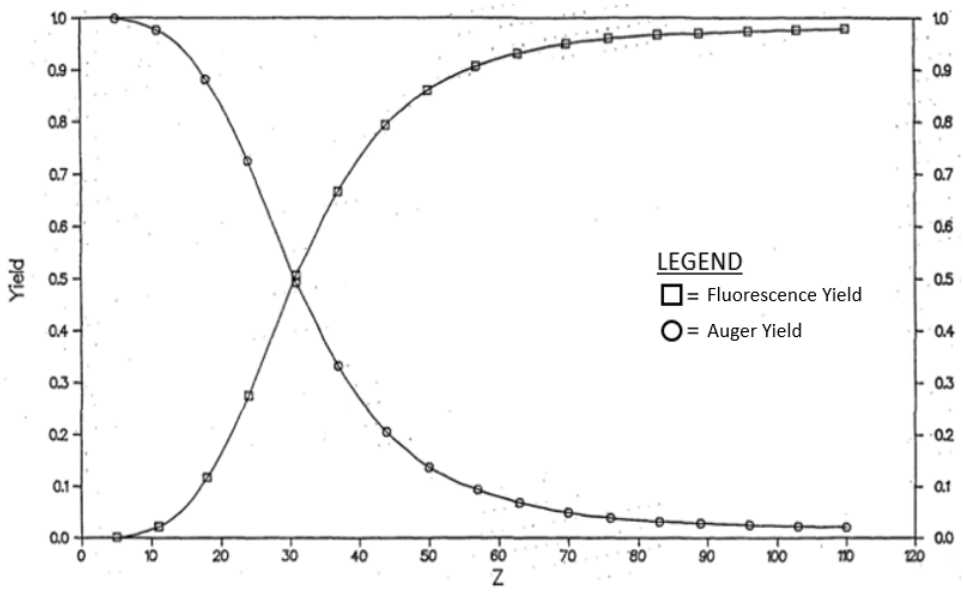

Figure 1-3: Relative yields for fluorescence and Auger electrons for K shell transitions. The bulk of X-PEEM signal is from secondary electrons produced by scattering of primary/Auger electrons. Figure modified from Krause[11] with permission.

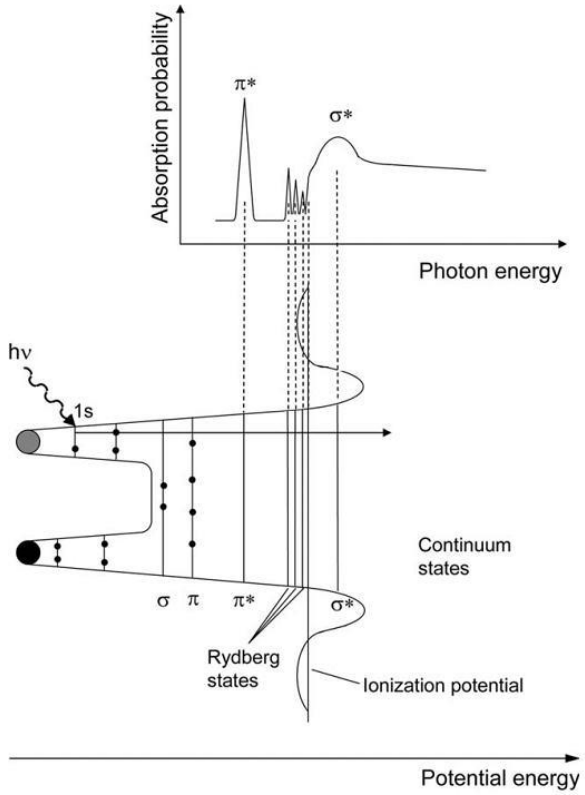

Figure 1-4: NEXAFS spectrum (top) and the corresponding molecular potential (bottom). Figure reprinted from Hahner[10] with permission.

Spectral structures in the NEXAFS region are dominated by multiple scattering contributions[8]. The energies that these transitions occur at and their shapes in the NEXAFS spectrum depend on the characteristics of excitation, as shown in Figure 1-4. These core electrons can be ionized from the atom, or excited into unoccupied π*, Rydberg, or σ* transitions. Rydberg peaks are atomic like transitions. They appear as low intensity, sharp peaks in the spectrum. The width and shape of spectral structures is determined by the lifetime of excited states, as given by the uncertainty principle

$$\Delta E \Delta t \leq \hbar/2 \qquad (1.1)$$

and therefore excited states with long lifetimes (and corresponding large Δt) give rise to sharper peaks in the NEXAFS spectrum (from a corresponding smaller ΔE). Long-lived π* transitions are sharp, whereas σ* transitions are shorter lived and are generally broader. The π* transitions occur below the ionization potential, whereas the σ* transitions usually occur above. Rydberg states always occur below the ionization potential. The broadening of the σ* peaks can also be caused by an increased possibility of decay to continuum states, due to an overlap of the σ* states and the continuum[8].

NEXAFS spectroscopy can be used to determine the elemental composition of a material. NEXAFS spectroscopy can also be used to study local environment of an element, such as functional groups and oxidation states[12]. When the material being studied exhibits a preferential ordering, orientation analysis can also be performed using polarized X-rays. The orientation analysis of molecules using polarized X-rays will be discussed in detail below.

1.1.2 Orientation Analysis with Polarized NEXAFS

Although the energy and intensity of a specific feature in a NEXAFS spectrum depends on the elements present and the local environment of these elements, the intensity of these transitions can also depend on the orientation of the TDM of specific electronic transitions in a molecule when linearly polarized X-rays are used. The polarization of light refers to the electric field vector ($\vec{\boldsymbol{E}}$) of the X-rays, as shown in Figure 1-5. When a material exhibits anisotropic absorption of X-ray radiation when linearly

polarized light is incident on it, this is called linear dichroism. This linear dichroism means that NEXAFS spectroscopy is sensitive to molecular orientation in ordered materials. Linear dichroism and orientation analysis using NEXAFS spectroscopy will be discussed below.

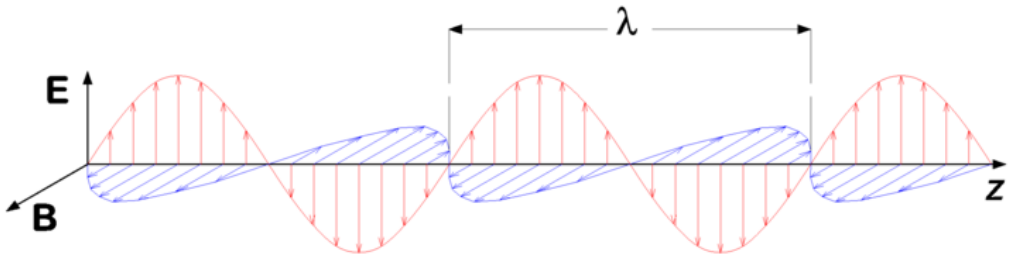

Figure 1-5: Illustration of an electromagnetic wave where the polarization vector (red) is oriented vertical. The magnetic field vector (blue) is always at a right angle to the electric field vector, and both are perpendicular to direction of propagation. CC BY-SA 3.0[13]

Features of NEXAFS spectra can exhibit linear dichroism in ordered samples. The electronic transitions that occur in X-ray absorption follow dipole selection rules. Absorption is strongest when the $\vec{\boldsymbol{E}}$ of the incoming linear polarized X-rays is aligned with the TDM. Equation 1.2 shows that the magnitude of absorption (I) is proportional to the angle (θ) between the $\vec{\boldsymbol{E}}$ and the TDM (μ_{if}),

$$I \propto |\vec{\boldsymbol{E}} \bullet \mu_{if}|^2 = \left|\vec{\boldsymbol{E}}\right|^2 |\mu_{if}|^2 cos^2\theta \quad (2.2)$$

where μ_{if} is the one-electron TDM from the initial to the final state. μ_{if} is defined as

$$\mu_{if} = \langle \psi_f | \mu | \psi_i \rangle \quad (1.3)$$

where μ is the dipole operator and ψ_f and ψ_i are the final and initial states, respectively. Therefore, the intensity of the transition depends on the orientation of the TDM relative to the direction of the $\vec{\boldsymbol{E}}$ of the polarized X-rays. In an absorption spectrum, light has a maximum probability of absorption when polarized parallel to the TDM, and a minimum probability when polarized perpendicular to the TDM.

The orientation of molecules on an ordered sample can be determined from the NEXAFS spectrum by using the polarization characteristics of synchrotron light. When there exists a preferential absorption of a specific polarization in the NEXAFS spectrum of a sample, the orientation of a specific TDM can be determined. When linear dichroism in NEXAFS spectroscopy is combined with the spatial resolution of PEEM, contrast differences appear between different orientations of TDMs within a molecule and the orientation of the molecule can be established. For saturated hydrocarbons, this information is gained by comparing angle dependent spectra of the C 1s → $\sigma^*_{C\text{-}C}$ and C 1s → $\sigma^*_{C\text{-}H}$ transitions, as discussed below.

1.1.3 X-ray Absorption Linear Dichroism of Hydrocarbons

NEXAFS spectroscopy is a useful technique for studying the molecular orientation of organic molecules. The core → π* transitions in unsaturated molecules are short lived, and therefore sharp peaks in the spectrum because the natural width of resonances is determined by the lifetime of the excited state[8]. The position of the π* transitions in the spectrum usually occurs below the ionization potential, leading to clear and uncluttered peaks in the NEXAFS spectrum. Figure 1-6 shows several NEXAFS spectra of highly oriented pyrolytic graphite (HOPG) with changing orientation between the $\vec{E}$ of the X-ray beam and the TDM of the molecular plane. HOPG represents an ideal sample as it is known that HOPG consists of layers of 6-membered benzene rings oriented parallel the substrate surface. It can be clearly seen that the intensity of the π* transition that occurs at 285 eV is strongest when the $\vec{E}$ of the X-ray beam is perpendicular to the graphite surface, while the intensity of the transition nearly vanishes when the $\vec{E}$ becomes parallel to the surface. As the TDM of the C 1s → π* is aligned perpendicular to the surface in the HOPG graphite sheets, the maximum intensity of the transition occurs when the $\vec{E}$ of the X-ray beam is also aligned perpendicular to the surface. This affirms that the graphite sheets are parallel to the surface.

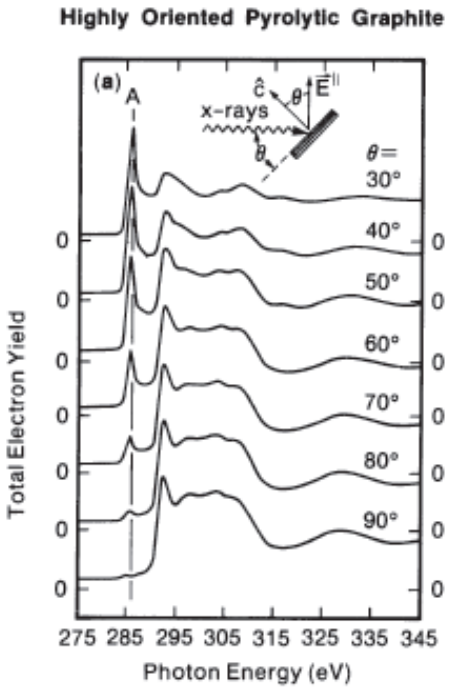

Figure 1-6: NEXAFS spectra of HOPG as a function of angle dependence of incident X-rays. Figure reprinted from Stohr[8] with permission.

Conversely, saturated molecules, such as *n*-alkanes contain no core → π* transitions that have well defined symmetry. For these systems, the core → σ* transitions must be used to determine molecular orientation. This is complicated by the σ* transitions occurring near the ionization potential, broadening the peak and causing difficulty in precisely determining the peak position. Figure 1-7 shows Carbon 1s NEXAFS spectra of a hexacontane ($C_{60}H_{122}$) thin film, deposited on a NaCl (001) surface, as a function of polarization angle. In this experiment, the sample is rotated about the beam axis to change the angle of polarization relative to the TDM of the sample. $\theta = 0^{o}$ and $\theta = 90^{o}$ are defined as the angles at which the intensity of the C 1s → $\sigma^*_{C\text{-}H}$ transition reaches minimum and maximum intensity, respectively. The C 1s → $\sigma^*_{C\text{-}H}$ transition (288 eV) shows the largest intensity when the $\vec{E}$ of the X-ray beam is oriented perpendicular to the alkane chain (in the CH_2 plane). At this polarization, the intensity of the C 1s → $\sigma^*_{C\text{-}C}$ transition (293 eV) will be supressed as the TDM is perpendicular to the $\vec{E}$ of the polarized X-ray beam. As the polarization angle is reduced and the $\vec{E}$ becomes aligned with the *n*-alkane backbone, the intensity of the $\sigma^*_{C\text{-}H}$ transition decreases, and conversely the $\sigma^*_{C\text{-}C}$ transition increases.

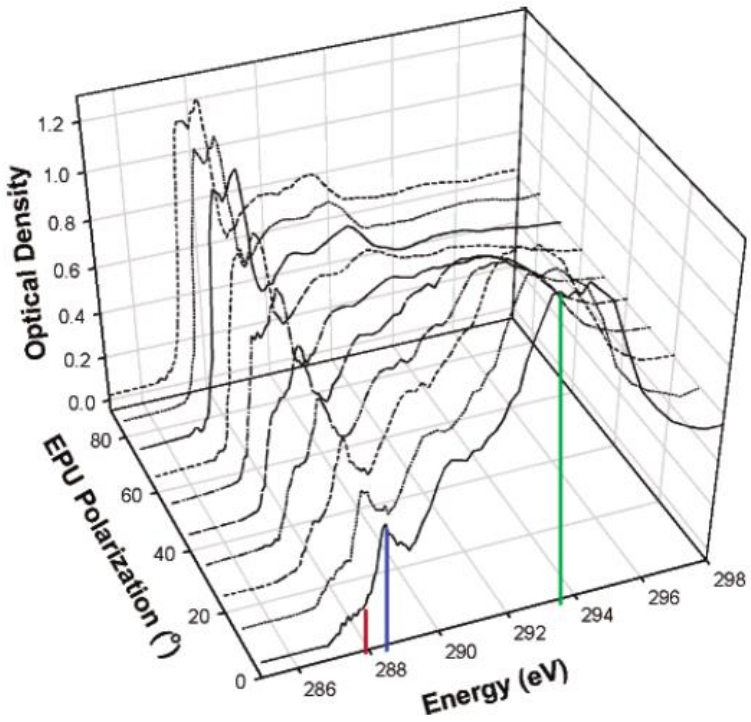

Figure 1-7: Carbon 1s NEXAFS spectra of an n-alkane thin film as a function of polarization angle. Figure reprinted from Fu *et al*.[7] with permission.

While polarized NEXAFS spectra provide information regarding the molecular orientation of thin ordered films, spatial recognition is needed to study films with separate ordered domains. When photoemission electron microscopy (PEEM) is combined with NEXAFS spectroscopy, chemical sensitive and orientation specific information can be obtained for specific areas of a sample with spatial resolutions down to 100 nm. The X-PEEM technique has been used to study molecular order in organic thin film systems, such as polyimines[14], alkane thiolate films on gold[15], and observation of pentacene film growth in real time[16], and many more examples. The following section will discuss the theory and principles of PEEM.

1.2 Photoemission Electron Microscopy (PEEM) – Theory and Technique

Photoemission electron microscopy (PEEM) is an electron microscopy technique where variations in the work function and topography of the surface create image contrast. With X-PEEM, X-rays are absorbed by the sample, exciting core electrons. A cascade of secondary electrons follows the

excitation of core electrons, which is generated by the inelastic scattering of primary and Auger electrons. The sample is held at a large negative potential, so electrons that escape the surface are accelerated from the sample and collected with a series of electromagnetic or magnetic lenses, as shown in Figure 1-8.

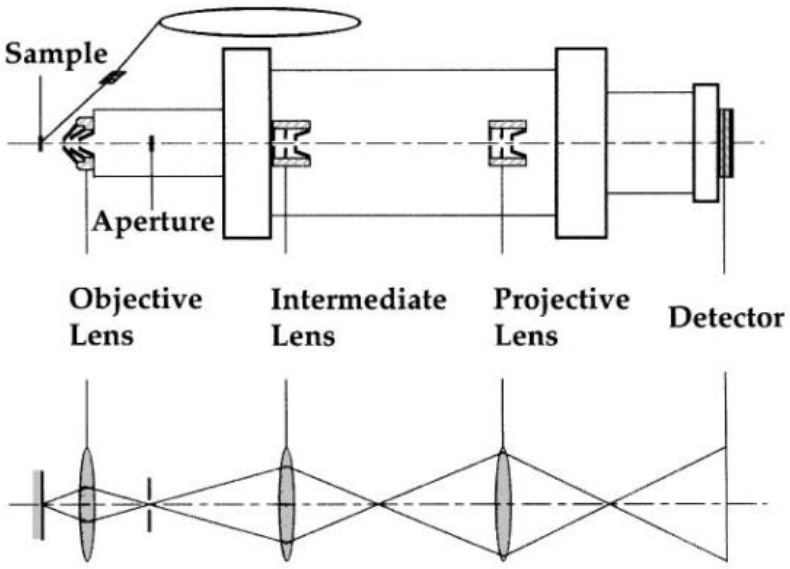

Figure 1-8: A basic schematic of electromagnetic lenses used in a PEEM. Figure reprinted from Gilbert *et al.*[17] with permission.

The contrast variations that appear on the image correspond to variations in the electron emission of the material. These variations can arise from the work function, photoemission cross-section, or surface topography of the materials. The majority of electron emission is dependent on the work function of the material, which is defined as the minimum energy required in order to remove an electron from a solid. A smaller work function then indicates there will be more electron emission, and therefore a brighter PEEM image. The work function for most elements lie between 3 and 5 eV. The work functions of some common elements, such as Au, Si, and Fe, are 5.37 eV, 4.85 eV, and 4.81 eV, respectively[18].

As with most electron microscopy techniques, PEEM samples must be conductive, stable under ultra-high vacuum (UHV) conditions, and free of large changes in surface topography. Samples that are not flat will cause field emission from topographical features on the surface. Figure 1-9(a) shows the effect of surface features on the corresponding image. The distortion of the electric field by topographical

features causes peaks to appear darker and valleys appear brighter when compared to flat regions[19]. Large surface features may also block illumination of areas in the features shadow. Sharp peaks can also cause field emission, causing focusing problems and image distortion[20].

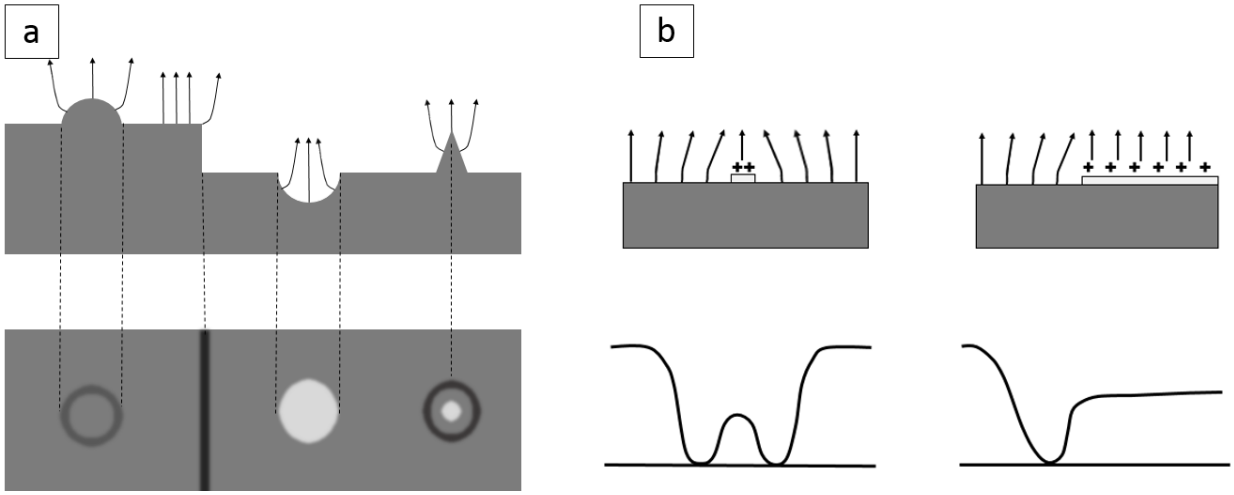

Figure 1-9: (a) Topological surface features (above) and the approximate corresponding PEEM image (below). (b) Effects of localized charging on a PEEM image (above) and the corresponding image intensity (below). Adapted from Gilbert *et al.*[17].

Nonconductive samples can cause charging effects and electrical discharges, as shown in Figure 1-9(b). This can cause focusing problems, and in extreme cases, electrical discharges may cause damage the MCP. Localized insulating areas on a sample can cause localized charge area that deflect the trajectories of the emitted electrons, causing images to become distorted[17].

Any light source that generates photons with sufficient energy to overcome the work function of the sample can be used for PEEM. The relationship between the maximum kinetic energy of the emitted electrons (K_{max}) is shown in the following equation.

$$K_{max} = hf - \varphi \quad (1.4)$$

In the equation above, φ represents the work function of the material, f is the frequency of the light interacting with the material, and h is the Planck constant. This equation shows that the kinetic energy of the electrons that are produced ranges from 0 to the energy of the incident photon, less the work function of the material.

The most common energy range of light used purely for imaging is ultraviolet (UV) light, as cost-effective bright sources such as Hg arc lamps are available, and UV light produces the highest resolution images. This is because lower energy light produces a smaller range on electron energies, lowering the amount of chromatic aberration in the image produced. Synchrotron produced X-rays are used when analytical information is required through NEXAFS, as synchrotron light can be tuned and images can be gathered at differing energies. The use of X-rays lowers the resolution somewhat however, as chromatic aberration is increased.

The X-rays illuminating the sample will penetrate the substance to a depth, known as the attenuation length, that is largely dependent on the on the density of the material and the photon energy. For any material, the attenuation length is defined as the distance (λ) where the probability of finding a photon has dropped to 1/e. In other words, it is the depth into a material where the intensity of the X-ray beam has been reduced to 63% (1/e). In general, the attenuation length is inversely proportional to the density of the material, but this is also dependent on the material's X-ray absorption properties. For example, the attenuation length for graphite (density = 2.2 g/cm^3) at 200 eV is approximately 1 μm, while the attenuation length of Cu (density = 8.96 g/cm^3) at 200 eV is approximately 30 nm[9].

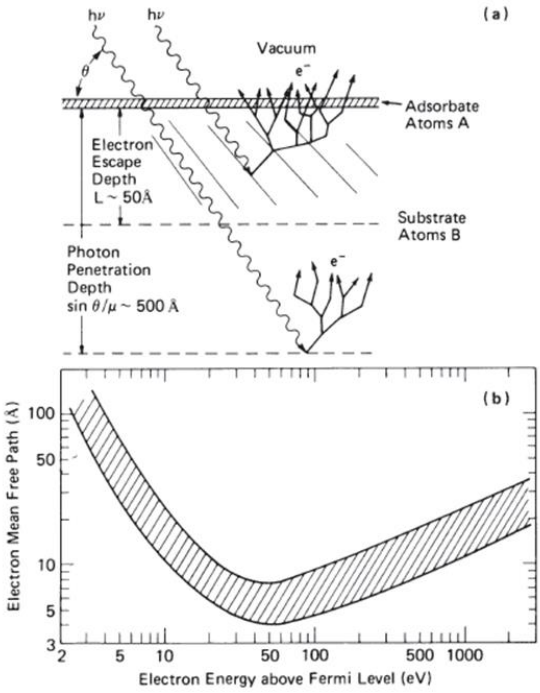

Figure 1-10: Photoabsorption and electron generation of a sample with a substrate layer B and adsorbate layer A. A universal curve for the mean free path of electrons in solids as a function of energy is shown as well. Figure reprinted from Stohr[8] with permission.

In addition to the ejection of primary electrons due to the photoelectric effect, the absorption of X-rays creates primary photoelectrons and Auger electrons, at the surface and throughout the sample where the X-rays penetrated. The scattering of these electrons within the sample leads to an electron cascade. As these electrons travel to the surface of the sample, they are scattered by interactions with other electrons on their way there, creating secondary electrons. The depth that X-rays penetrate the sample to much greater than the depth of the electrons that escape the sample, owing to the small inelastic mean free path (λ) of the electrons generated. The λ of these electrons follows the universal curve, shown in Figure 1-10. As shown above, electrons with kinetic energies from 10-500 eV (typical for soft X-rays) have a small λ[21]. Therefore, the λ of electrons generated are generally by soft X-rays are typically below 10 Å. For example, the maximum probing depth of for Auger electrons with an energy below 500 eV is less than 5 nm[22]. Thus the electrons used for imaging in PEEM usually come from near the surface, giving PEEM excellent surface sensitivity.

Since the absorption of the illuminating light is dependent on the X-rays energy, contrast changes can be seen in PEEM images at different illumination energies. If an image of the sample is taken when illuminated at different wavelengths of monochromatic light, a series of images will be obtained that will allow changes in absorption to be observed with changing photon energies. This series of images allows a chemical and orientation sensitive NEXAFS spectrum to be acquired from specific areas of the sample where element specific information can be obtained. Synchrotron radiation also allows adjustable polarization, which give a great advantage for measuring molecular orientation on a surface[10, 14, 23].

The magnified electrons are amplified and detected using a micro-channel plate (MCP)/phosphor combination. The MCP consists of many small channels typically 10μm in size, although high resolution MCPs may have channels as small as 0.4 μm[24]. These channels are densely distributed over the surface of the MCP and function independently as electron multipliers. The MCP amplifies the electrons by producing a cascade when one electron strikes the sidewalls of the MCP channels. In this way the MCP amplifies the electron signal while maintaining the spatial resolution of the electrons. The phosphor screen generates visible light when the electron pulse strikes it. The phosphor is viewed with a cooled charge coupled device (CCD) camera.

PEEM is a powerful technique for studying the growth of thin films[16, 25]. When combined with polarized synchrotron light, PEEM can be used to record spatially resolved NEXAFS spectra where orientation of discrete areas of a sample can be determined[14]. This technique is particularly useful for samples with molecular ordering, as information regarding the elemental composition and orientation can be determined for specific areas of a heterogeneous sample. In the following sections, the mechanisms behind the growth of ordered thin films will be discussed.

1.3 Growth of Organic Thin Films

n-alkane films may be prepared in a highly ordered arrangement when grown on crystalline substrates. The process of depositing an ordered crystalline overlayer on a crystalline substrate is known

as epitaxy. Epitaxy is a form of crystal growth that exists as a nucleation and growth relationship between two crystalline phases. This allows a crystalline phase (epitaxial layer) to be grown on another crystalline phase (substrate layer) that is dependent on the structure on the substrate layer. The epitaxial layer can be formed from many different sources, including liquids, vapours, or molecular and atomic beams[26]. These surfaces grown by epitaxy can be directly observed by several methods, such as AFM, scanning transmission X-ray microscopy (STXM), scanning electron microscopy (SEM), and PEEM, among others.

When the epitaxial layer is grown on a substrate with a well-defined crystal phase, the crystal structure of the grown layer may conform to that of the substrate, even if there is a significant lattice mismatch between the substrate crystal phase and the most thermodynamically favourable crystal structure of the deposit[26]. The study of epitaxial adsorbed organic molecules of a film is an important method to study surfaces. Small changes to the substrate, such as surface defects or impurities, can have a significant influence on the growth of adsorbing molecules. The basics of epitaxial growth and how this applies to long chain molecules will be discussed below.

1.3.1 Atomic Epitaxy

Epitaxy is the process of film growth where atoms of the growing film, known as the epilayer, mimic the arrangement of the atoms of the substrate that the film is growing on[26]. During epitaxial growth, the adsorbing molecules are transported to the surface of the substrate, and crystalline growth occurs at the interface between these two phases. It is important for the interfacial area to remain in a supersaturation state with the adsorbing molecules, as epitaxial growth cannot occur otherwise. The epitaxial growth process as a process of atomic ordering, which is strongly dependent on the chemical activity of the substrate surface, as well as the kinetics of the process[26].

Figure 1-11: The three different growth modes; Frank-van de Merwe (left), Volmer-Weber mode (center), and Stranski-Krastanov (right). Figure adapted from Herman *et al.*[26] with permission.

The growth processes of epitaxial films occur similarly to bulk crystal growth, with the exception of the influence of the substrate on the initial stages of growth[26]. There are five possible growth modes in which epitaxial growth can occur. These are Volmer-Weber mode, Frank-van der Merwe mode, Stransk-Krastanov mode, columnar growth mode, and step flow mode[27]. The three most common modes of epitaxial growth are depicted in Figure 1-11. These are Frank-van de Merwe mode, Volmer-Weber mode, and Stranski-Krastanov mode. In Frank-van der Merwe mode, the substance grows layer-by-layer on the substrate, where an entire monolayer forms before new growth begins on top. This will happen when the adsorbing atoms or molecules have a larger affinity for the substrate than for each other. In Volmer-Weber mode, islands form when incoming atoms or molecules form small clusters and then grow larger. This growth mode will occur when the adsorbing atoms or molecules have a larger affinity for each other than for the substrate. The Stranski-Krastanov mode is an intermediate growth mode, between the Frank-van de Merwe and Volmer-Weber modes. This growth mode will occur when the adsorbing molecules or atoms completely cover the surface and subsequent layers have a decreasing attraction to the substrate. Eventually the adsorbing atoms or molecules will have a greater affinity to each other than to the substrate and islands will form.

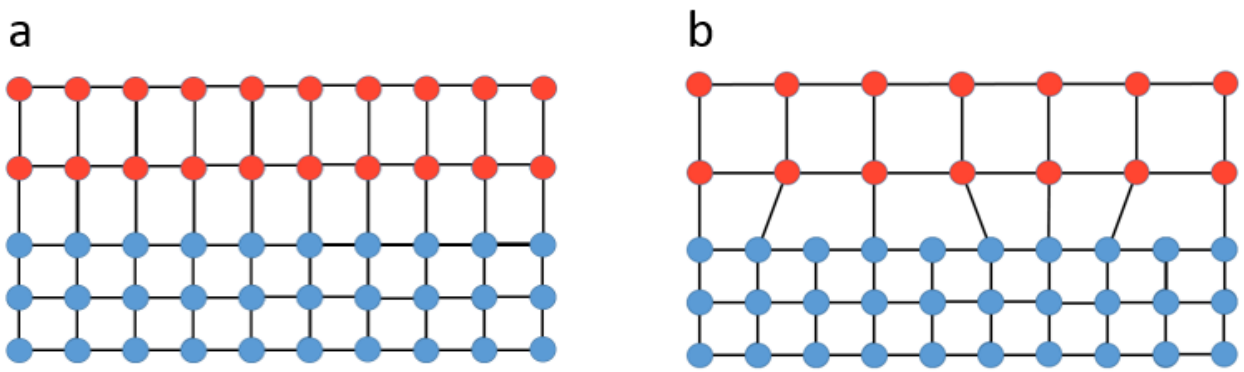

Figure 1-12: Illustration of a strained epitaxial layer (a) and a relaxed epitaxial layer (b). Adapted from Herman *et al.*[26].

If the lattices of the epilayer and the substrate are mismatched, the lattice of the epilayer will become distorted to accommodate this misfit. The lattice of the epilayer may become strained as it distorts to conform to the lattice of the substrate Figure 1-12a, or the lattice of the epilayer may distort through relaxation Figure 1-12b. If the misfit between the substrate and epilayer is small, the first monolayers that are deposited will be strained to match the substrate. As the thickness increases however, the energy required to strain the lattice may become large enough that is energetically favourable for the epilayer to relax and introduce dislocations[26]. This is the case for Stranski-Krastanov growth.

1.3.2 Molecular Epitaxy

In contrast to atomic epitaxy, epitaxy with molecules introduces addition variables and complexities. Large molecules may have differing degrees of commensurism with the substrate, where the epitaxial layer may closely match lattice points on the substrate (commensurate), or may only have very little in common with the substrate (incommensurate). Commensurate and incommensurate molecular epitaxy of large molecules can lead to preferential orientations in thin films, as discussed below.

In order for molecular epitaxial growth to occur, the overlayer must have a commensurate configuration with the lattice points of the substrate layer. For epitaxy of large molecules, this can be

satisfied by varying degrees of commensurism, such as point on point coincidence where for high degrees of commensuism, to point on line for lower degrees. These two forms of commensurism are shown in Figure 1-13. Point-on-point commensurism occurs where each lattice point of the over layer matches directly with a point of the substrate. Lattice lines of the over layer must also coincide with lattice lines of the substrate. For point-on-line commensurism, the lattice points of the over layer do not coincide with all lattice points on the substrate, but every lattice point coincides with a lattice line of the substrate[28].

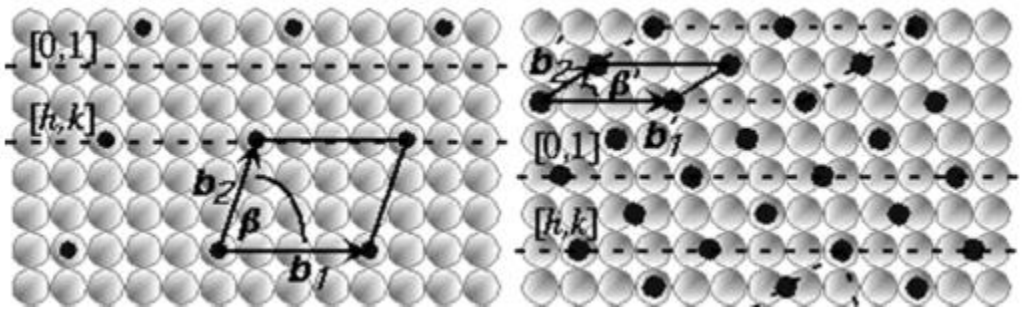

Figure 1-13: A representation of point-on-point (left) and point-on-line commensurism (right) molecular epitaxy. The larger white circles represent the substrate, while the smaller black circles represent the deposited layer. Figure modified from Hooks *et al.*[28] with permission.

Epitaxial growth can also occur incommensurately. For an incommensurate over layer, there exists a preferred orientation of growth, even though there does not exist any distinct matching between lattice lines of the over layer and substrate. For example, a film of hexabrobobenzene (C_6Br_6) grown on graphite exhibits a unique orientation, even though the lattice constants for graphite and C_6Br_6 are very different (2.46 Å and 9.14 Å, respectively)[28]. The ability for a substrate to distort the growth of an over layer from its natural order depends on the degree of fit between the two lattices.

The epitaxial growth of *n*-alkanes occurs by following energetically favourable directions on several surfaces. Of particular interest is growth on HOPG (0001) and single crystalline NaCl (001) surfaces, where films grow in six-fold and four-fold symmetry, respectively[29]. The process in which this occurs is complex however and dependent on many variables. This work will explore the details of this growth in more depth to attempt to provide an explanation for the growth mechanisms.

1.4 Previous Study of *n*-alkanes on High Symmetry Surfaces

The way a substance grows on a surface is dependent on many conditions, including substrate temperature, substrate heat capacity, deposition rate, as well as others. When *n*-alkanes are epitaxially grown on a highly ordered substrate, a series of complex orientational morphologies are observed that depend on the deposition conditions. By using PEEM and NEXAFS, the early stage growth of *n*-alkane films can be studied in detail.

1.4.1 Molecular Orientation of *n*-alkanes

Two fundamental molecular orientations have been identified for the growth of *n*-alkanes in all-trans configuration on high symmetry substrates. These are lateral, where the carbon backbone is aligned parallel to the surface, and normal, where the backbone is aligned perpendicular to the surface[30]. Laterally oriented *n*-alkanes may also be oriented side-on, where the carbon chain zig zags parallel to the plane of the substrate, on or edge on, where the carbon chain zig zags are perpendicular to the substrate plane. The differences between side on and edge on orientations are shown visually in Figure 1-14

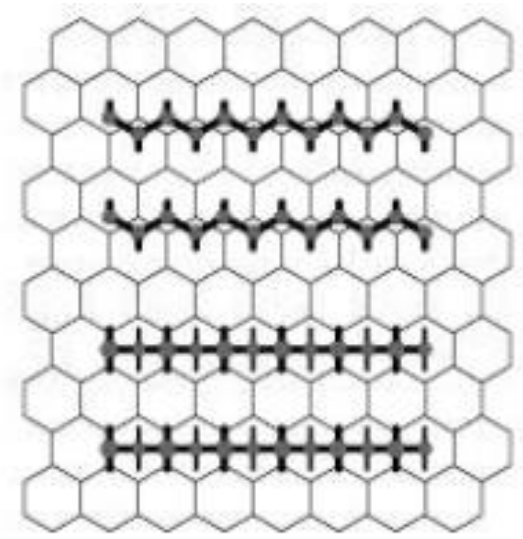

Figure 1-14: Two possible variations of laterally oriented n-alkane chains, where the backbone of the carbon chain is oriented parallel to the to the plane of the substrate (above) and where the backbone is oriented perpendicular to the plane of the substrate (below). Figure modified from Leunissen *et al.*[31] with permission.

Thin *n*-alkane films are often prepared through physical vapour deposition (PVD). PVD is a widely used technique for depositing thin films for various solid sources. In PVD, the chemical to be grown is transported to the substrate in the vapour phase, without chemical change. Compounds or elements are sublimed or vapourized by resistive heating or laser ablation. PVD allows for the controlling of growth parameters, such as deposition rate, angle, substrate temperature, and kinetic energy of the vapour phase that are unable to be controlled in other techniques, such as solution deposition. These parameters are important to control because they influence the adsorption and desorption processes.

PVD is often done in vacuum to reduce the chance of impurities being included in the grown layers. Vacuum evaporation also creates the possibility of *in situ* techniques to be applied during film growth, although not all *in situ* techniques are UHV compatible. Among the most important factors governing the growth of *n*-alkane films from vapours in vacuum conditions are the substrate temperature and the deposition rate[32].

A simple model proposed by Kubono *et al*.[32] is described here, where initial growth occurs in several steps. Figure 1-15 gives a schematic representation of these steps. When molecules that form ordered thin films first interact with the surface they are being adsorbed to (1), the molecules will migrate across the surface (2). The molecules may either re-evaporate from the surface (3), or cluster together and orient themselves from a random orientation to form an ordered nucleation site (4). As the molecules form nucleation clusters, they may re-evaporate from the cluster (5), or reorient themselves to their preferred orientation (6). The conditions at which this process takes place are important to consider, as they have a large influence on the observed morphologies of the film that is grown. Of particular importance are the substrate temperature and the deposition rate.

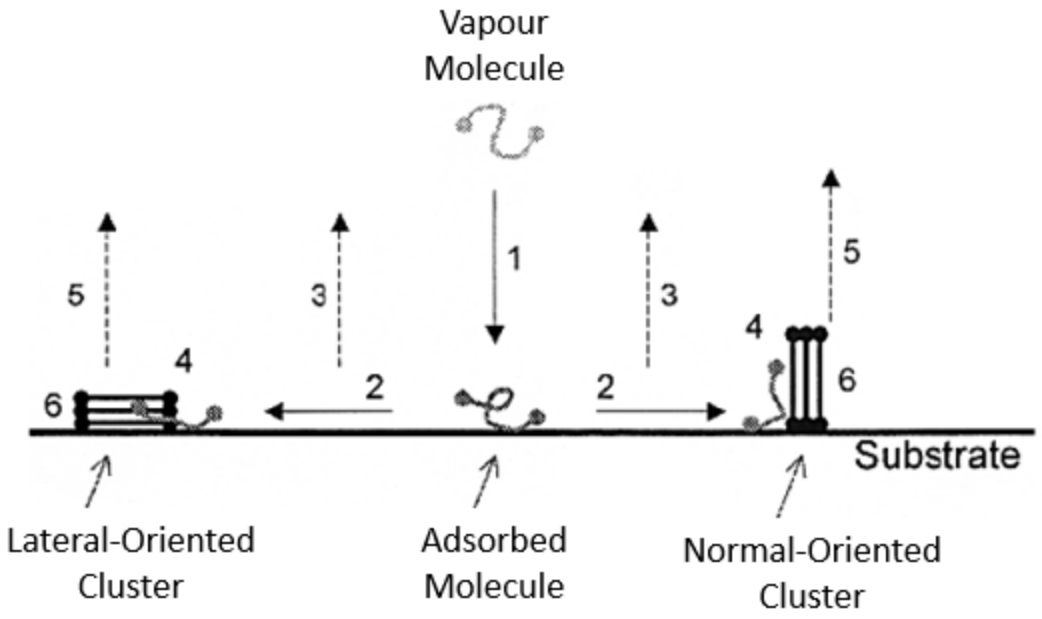

Figure 1-15: Illustration of thin film growth. Adsorption from vapour (1), surface migration (2), re-evaporation from surface (3), capture into oriented cluster (4), re-evaporation from cluster (5), reorientation (6). Figure modified from Kubono *et al.*[32] with permission.

Substrate temperature plays an important role in the evaporation and re-evaporation of molecules from the substrate, as a higher substrate temperature will increase the energy of the adsorbed molecules. This can cause the molecules to have greater re-evaporation rates from the substrate, greater ability to migrate along the surface of the substrate, and a greater ability to reorient. Figure 1-16 shows the percentage of normally oriented clusters as a function of substrate temperature for $C_{40}H_{82}$ deposited on glass by PVD[33]. The method used to determine the orientation of the alkane clusters was X-ray diffraction, which does not have spatial resolution for this example. As a consequence, the orientation measurements give the average of the entire film. The normally oriented clusters are formed at higher temperatures, while the lateral orientated clusters are formed at lower substrate temperatures. In the $C_{40}H_{82}$ example below, the equilibrium temperature, where half the $C_{40}H_{82}$ molecules are oriented normal to the substrate and half are in the lateral orientation, is 270K. The lateral orientation provides an increase in surface area, leading to higher rates of evaporation and re-evaporation from the substrate[23]. This in turn leads to the lateral orientation being found at lower substrate temperatures.

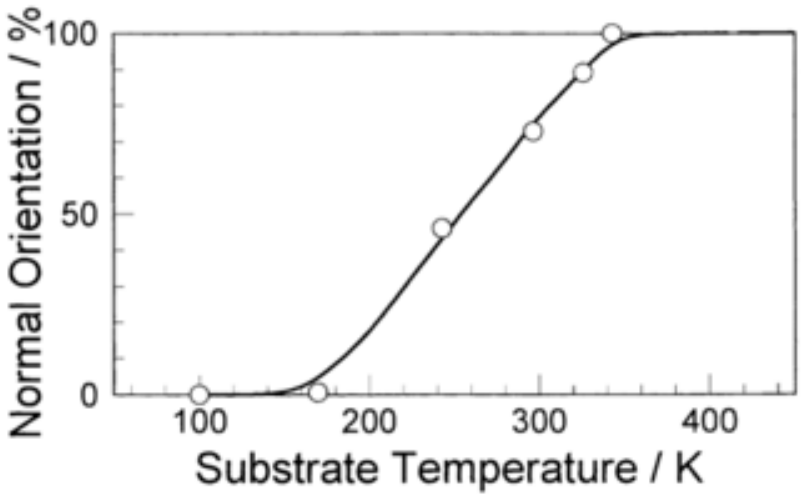

Figure 1-16: Percentage of normal orientated $C_{40}H_{82}$ molecules on glass as a function of temperature. Figure Modified from Kubono *et al.*[32] with permission.

The rate of deposition also influences the growth of ordered thin films[32]. At higher deposition rate, re-evaporation from the surface and from cluster will be reduced, and *n*-alkane molecules will prefer the lateral orientation. This is due to a larger interaction of the molecule with the substrate surface from the greater contact area of the laterally oriented molecule compared to the normal orientation[32]. When the rate of molecules reaching the surface increases, nucleated clusters grow faster. This means that molecules do not need to migrate as far across the surface as far before joining clusters, and will not have time to re-evaporate and rearrange before more molecules adsorb. Consequently, a film grown at a slower deposition rate will prefer the normally oriented clusters, while a film grown with a higher deposition rate will preferentially form laterally oriented clusters.

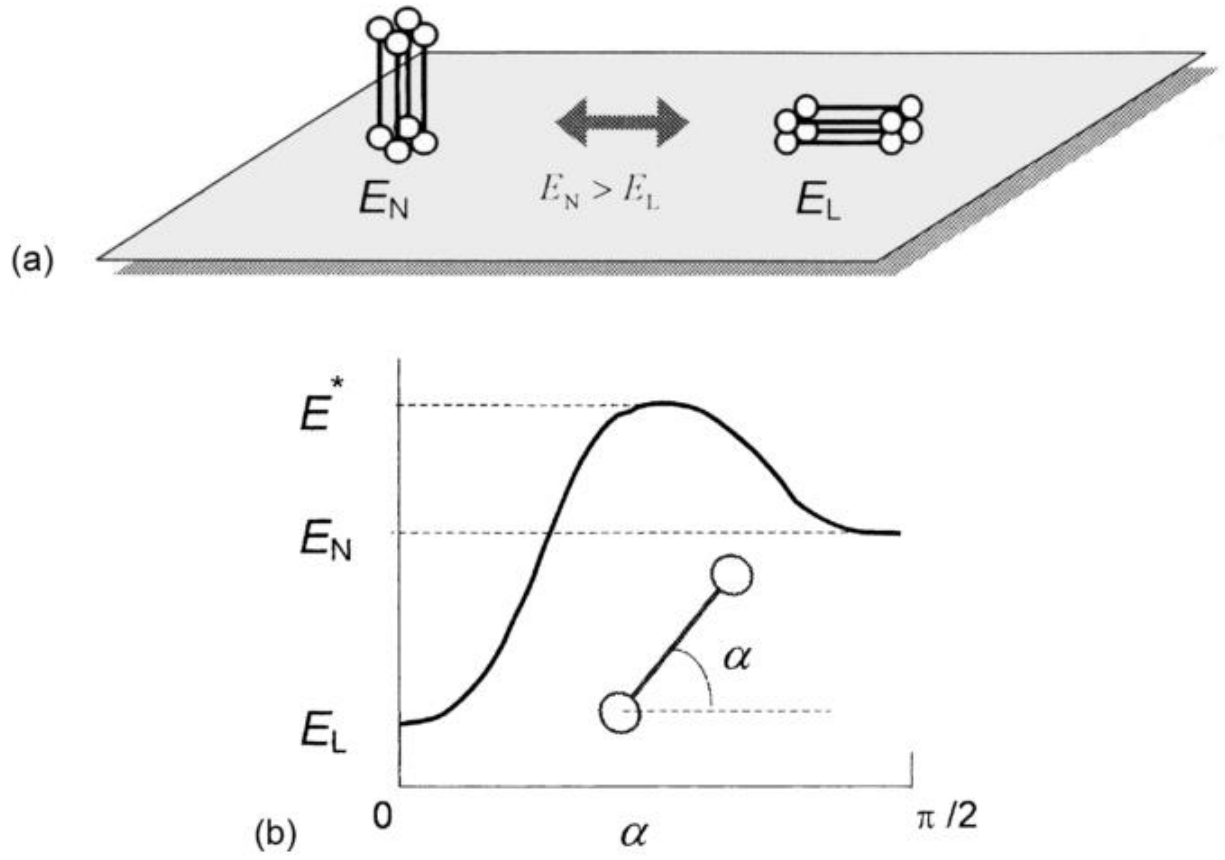

Figure 1-17: Normal and lateral orientations of n-alkane nuclei (a). Potential energy as a function of molecular tilt angle of the molecule (b). Figure reprinted from Kubono *et al.*[32] with permission.

The dependence or orientation can also be described thermodynamically[30]. Normally oriented clusters have a larger potential energy compared to the lateral clusters, and therefore the lateral orientation is preferred to normal orientation. Figure 1-17 shows the potential energy of the *n*-alkane clusters as a function of molecular tilt angle. The two orientations are stable with the normal orientation at higher temperatures being preferred. The preferred orientation of *n*-alkane thin films cannot be described in purely thermodynamic terms. The degrees of freedom for clusters of normal or laterally oriented molecules should similar, so it is assumed that entropy is independent of molecular orientation[32]. Therefore, the driving force behind the growth of oriented *n*-alkane thin films is the relative rate of the formation of nucleation sites for the normal and laterally oriented clusters. This is dependent on the critical nucleus sizes for each orientation, as well as the temperature of the substrate[30].

When *n*-alkanes are deposited on a structured surface such as NaCl (001) or HOPG (0001), the observed films can grow epitaxially with an orientation that is commensurate with the substrate beneath. Leunissen *et al*. found that a complete monolayer of dotriacontane ($C_{32}H_{66}$) forms on the HOPG substrate (substrate temperature = 45°C) before islands nucleate on the monolayer[31]. Using a combination of polarization microscopy and AFM, Leuinissen *et al* determined that these islands are of the same orthorhombic crystal structure as the monolayer, with the carbon backbone of the molecules oriented parallel to the surface with a face on configuration. This configuration is not the most thermodynamically stable crystal structure of *n*-alkanes however. This suggests that the monolayer acts as a template, where three dimensional epitaxial nucleation occurs on the monolayer. In this case, the Stranski-Krastanov growth model that is observed is likely as a result of the large lattice mismatch between the HOPG substrate (4.2Å) and the alkane crystal phase (5.0Å).

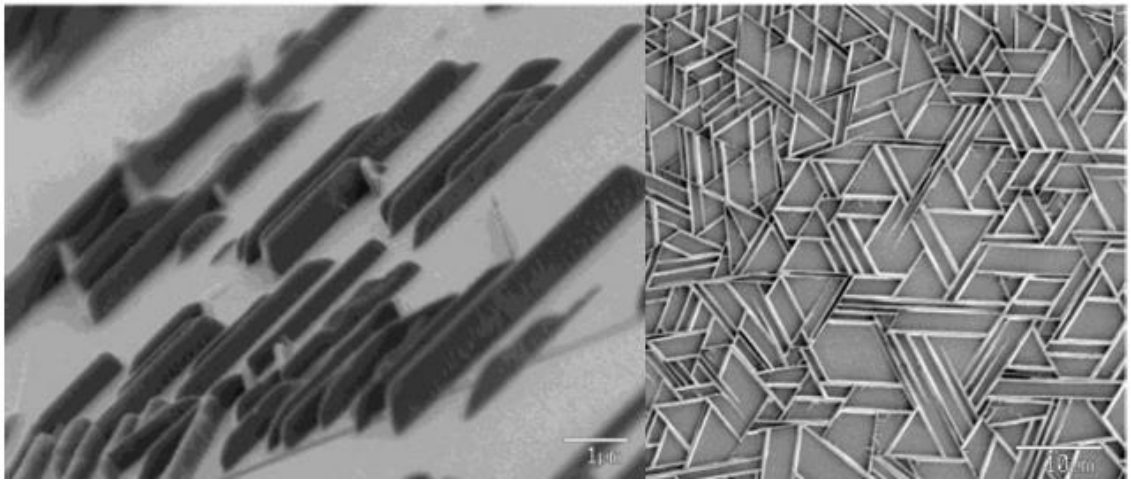

Figure 1-18: cryogenic scanning electron microscopy images of C32 on HOPG. Island growth can be seen in the tilted left image and six-fold symmetry can be seen in the rightmost image. Figure reprinted from Leunissen *et al.*[31] with permission.

In addition to the differences in molecular orientation, thin *n*-alkane films also show complex orientational morphologies when grown epitaxially on an ordered substrate. Figure 1-18 shows cryogenic scanning electron microscopy images of dotriacontane ($C_{32}H_{66}$, C32) on HOPG substrate. The rightmost image clearly shows the six-fold symmetry of *n*-alkane island growth on HOPG. The leftmost image is

taken from an angle and island growth can clearly be seen. After nucleation, the crystals expand parallel to the substrate until they reach another crystallite. The result is a trigonal pattern with orientations of islands at 60 degrees to each other, with edges almost perpendicular to the substrate surface. The morphology that is observed depends on the conditions during deposition, primarily on the substrate temperature. By creating *n*-alkane films at different substrate temperatures, the observed patterns can be tuned to a specific morphology. Previous studies of the morphological dependence on substrate temperature will be discussed in the following section.

1.4.2 Growth Patterns of *n*-alkane Films on HOPG at Different Substrate Temperatures

The patterns formed by *n*-alkanes grown on HOPG by physical vapour deposition show a large dependence on the temperature of the substrate when they are deposited[34]. There are several morphologies observed for *n*-alkanes based on several factors, including the length of the carbon chains, the rate of deposition, and the temperature of the substrate when deposited. By adjusting the temperature of the substrate during deposition, it is possible to control the morphology of the deposited *n*-alkane. Masnadi and Urquhart studied this temperature dependence in detail by varying the temperature of the substrate for multiple different *n*-alkane chain lengths[34]. The term "supercooling" is used to describe the variation of substrate temperature to normalize for the differences in *n*-alkane chain lengths, since alkanes with longer carbon chains have higher melting points than their short chain counterparts. The supercooling term (T_{SC}) is defined as the difference between the melting point of the *n*-alkane (T_{fus}) and the substrate temperature (T_S), shown in equation 1.5:

$$T_{SC} = T_{fus} - T_S \qquad (1.5)$$

Figure 1-19 shows the differing morphologies for hexatricontane ($C_{36}H_{74}$, C36) on HOPG at differing temperatures. At high supercooling temperatures, a flat film with uniform thickness and large domains is observed (a). As the supercooling temperature is decreased, distinct narrow bars appear (b) that increase in width and clearly show a six-fold symmetry as the supercooling temperature is further

decreased (c). A supercooling temperature between 20 °C and 25 °C gives rise to very thick bar structures ordered in a six-fold symmetry (d). After this point however the six-fold symmetry is no longer observed, and a morphology of large pseudo-rectangular domains is seen (e). At substrate temperatures close to the melting point of the *n*-alkane being deposited, a flat film with pseudo-rectangular domains is observed (f).

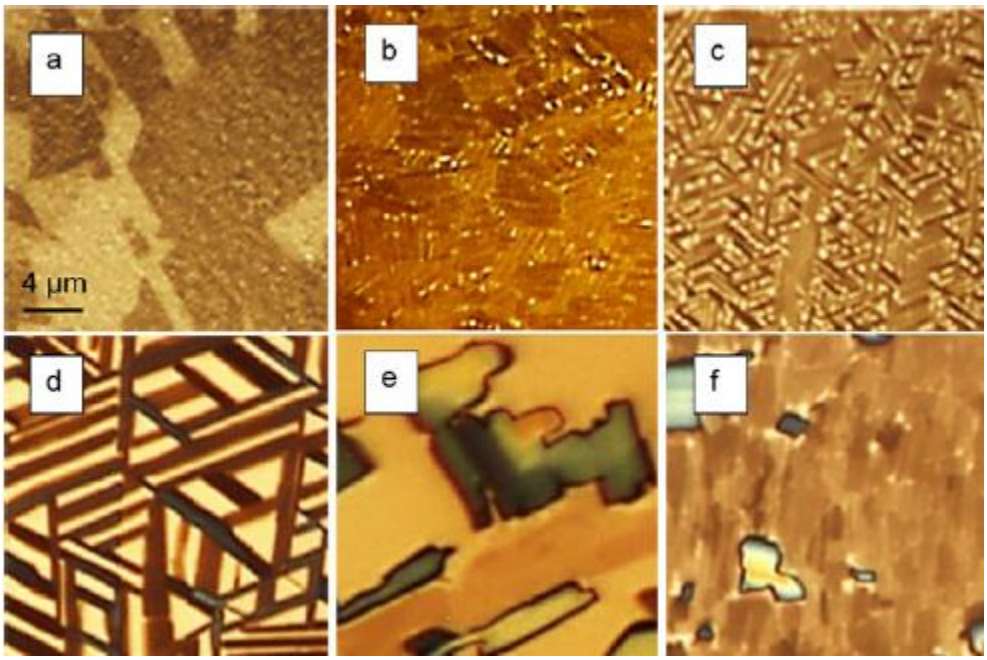

Figure 1-19: Optical microscope images of morphologies for C36 at different supercooling temperatures: (a) 6 °C(T_{SC}= 69.8 °C); (b) 25 °C(T_{SC} = 50.8 °C); (c) 30 °C(T_{SC} = 45.8 °C); (d) 50 °C(T_{SC} = 25.8 °C); (e) 56 °C(T_{SC}= 19.8 °C); (f) 65 °C(T_{SC}= 10.8 °C). Figure reprinted from Masnadi *et al.*[29] with permission.

A transition from layer growth to island growth is also observed during the growth of *n*-alkanes, suggesting a Stranski-Krastanov growth mode. This can be observed from *Figure 1-19*, where at low T_{SC} large islands without bars of six-fold symmetry are seen (a). At slightly higher T_{SC} large islands with small bars of six-fold symmetry are seen (b). This suggests a transition from layer growth to island growth of ordered domains. There are many possible reasons for Stranski-Krastanov growth to occur, as any factor that changes the binding energy may be the cause[26]. One possibility is to this growth mechanism change is strain, as strain in the grown film is often attributed to the Stranski-Krastanov growth mode. Initial deposition leads to the formation of one or more strained layers, whose structure is strongly influenced by the underlying substrate[27].

Care must be taken when discussing molecular epitaxy of *n*-alkanes, as there are a wider range of growth conditions (chain length, substrate temperature, evaporation rate, etc.) that have more importance than strain on the morphology of the prepared films[34]. It is important to understand the factors that affect the growth of *n*-alkane films in order to engineer films of a specific orientation.

As shown above, the epitaxial growth of *n*-alkane films on highly ordered surfaces depends on the conditions during growth. Small changes to the substrate temperature or evaporation rate can have a large influence on the type of complex morphology observed in the *n*-alkane film. In addition to the overall structure of the *n*-alkane film dependent on the growth conditions, the orientation of the carbon backbone of the molecules can vary from normally oriented to parallel, and side or edge-on orientation when parallel to the surface (see section 1.1.2.). In order to study these morphological differences in *n*-alkane films, a technique needs to be used that provides the spatial resolution necessary to observe *n*-alkane domains, but also provide information about the orientation of the constituent molecules as well. To this end, NEXAFS and PEEM will be used to study the growth of *n*-alkane films.

1.4.3 NEXAFS of *n*-alkanes

Imaging techniques such as AFM and SEM can be used to gain insight into the growth and orientation of thin films. Information about molecular orientations and growth cannot easily be directly observed with these techniques however. While X-ray diffraction techniques can give information about the orientation of crystallites, obtaining spatial resolution with such techniques is difficult however. By using polarized NEXAFS however, element specific information about molecular orientation can be directly discerned from spectra generated at discrete areas of a film.

NEXAFS spectroscopy is an excellent technique for studying the molecular orientation of *n*-alkane films. Core level excitations for low Z elements, such as carbon and oxygen, are well defined and occur in the soft X-ray energy region. The features of a NEXAFS spectrum are often presented in regards to these core level electron transitions to unoccupied valence orbitals with σ^* or π^* symmetry. These

features of the NEXAFS spectrum can give information about chemical composition[12, 35], local environment of the element under investigation[36], and the orientation of species adsorbed to a surface[10, 37].

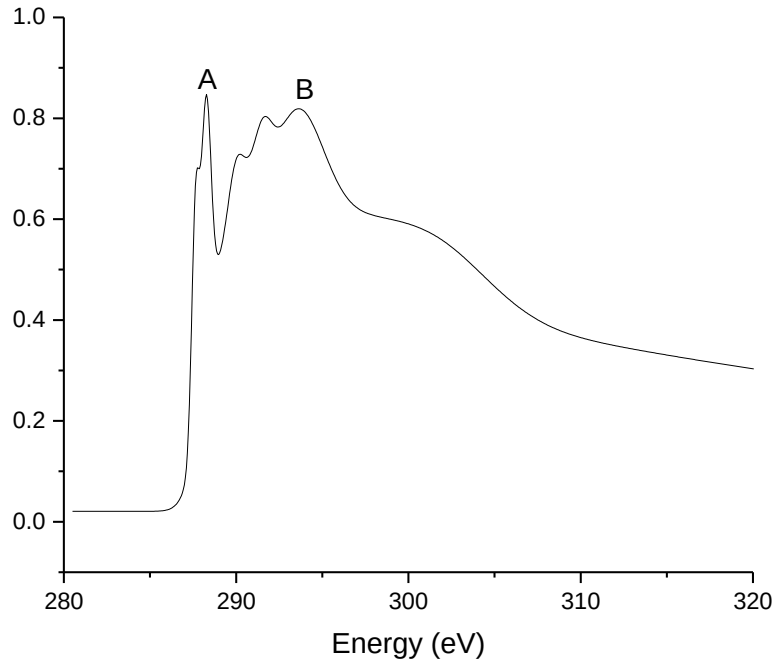

Figure 1-20: NEXAFS spectrum of hexacontane ($C_{60}H_{122}$). Spectra for saturated hydrocarbons are dominated by two resonances, the $\sigma^*_{(C-H)}$ and the $\sigma^*_{(C-C)}$ transitions, labelled A and B, respectively. Figure modified from Stohr[8] with permission.

Since *n*-alkanes are saturated molecules, there will be no π^* transitions observed in their NEXAFS spectrum. Consequently, the spectra of saturated hydrocarbons are dominated by two resonances: the $\sigma^*_{(C-H)}$ transition and the $\sigma^*_{(C-C)}$ transition, as shown in Figure 1-20. The energies that the $\sigma^*_{(C-H)}$ and $\sigma^*_{(C-C)}$ transitions occur at for *n*-alkanes typically occur at 288 eV and 293 eV. The $\sigma^*_{(C-H)}$ transition is a relatively sharp peak when compared to the $\sigma^*_{(C-C)}$ transition, which occurs near the ionization potential of *n*-alkanes, which leads to mixing with the continuum of the spectrum and broadening of the peak.

The intensities of the σ* transitions described above are dependent on the polarization of X-ray radiation used in samples that exhibit a preferential ordering. When the $\vec{E}$ of the X-rays is oriented along the chain direction of the *n*-alkane, the C-C transition at 293 eV is the most pronounced feature of the spectrum. Conversely, when the $\vec{E}$ of the X-rays is in line with the C-H transition, the peak at 288 eV will be most pronounced. The change in the intensities of these two peaks with the changing of polarization angle is clearly seen in Figure 1-7. The relationship between these peak intensities and the polarization angle allows the direction of carbon chains on an oriented sample to be determined.

A comparison of two C36 spectra recorded with polarized X-rays of two different orientations is given in Figure 1-21. The change in intensities of the C-H bands (287.5 eV) and the C-C bands (293 eV) provide information about the orientation of the alkane chains. This intensity change of the spectral features indicates that the carbon chains are oriented parallel to the surface, with their carbon backbone in plane with the substrate[34].

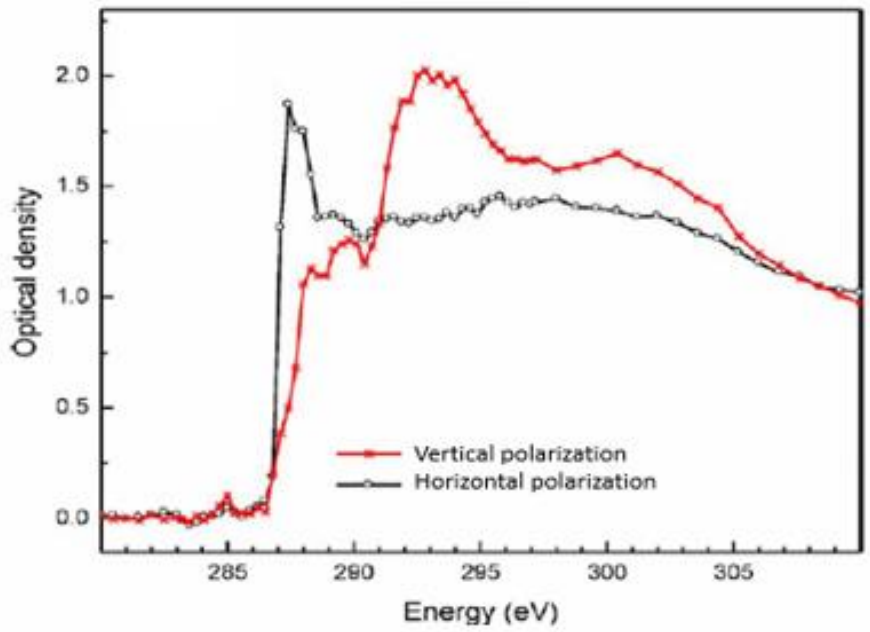

Figure 1-21: Spectra of a C36 on graphene sample recorded with vertical and horizontal polarizations. Figure modified from Masnadi *et al.*[34] with permission.

When NEXAFS spectra of oriented samples are collected with a technique such as STXM or PEEM, information about the orientation of specific domains can also be extracted. Figure 1-22 shows a STXM image of several different oriented bar structures (a) recorded at 288.2 eV of a sample of C36 deposited on graphene. The spectra correspond to the dark area labeled 1 (b) and the dark vertical bars (c). The spectrum of area 1 (b) indicates an *n*-alkane film where the carbon chains are oriented normal to the graphene surface. The spectrum shows an absorption maximum at 288 eV for both polarizations, indicating that the polarization is aligned along the C-H transition dipole moment for both spectra. The spectra for the vertical bars (c) show a variation in the intensity of the C-H and C-C bands however, indicating that these areas feature the alkane chains oriented parallel to the substrate surface. The continuum region of the spectrum for the parallel bar regions show a larger optical density than the normal oriented regions (approximately 0.4 vs 0.2, respectively) indication that the bar regions of the sample are thicker. These result show a mixture of parallel domains oriented normal to the surface, and *n*-alkane molecules in the islands orientated in the substrate plane[34].

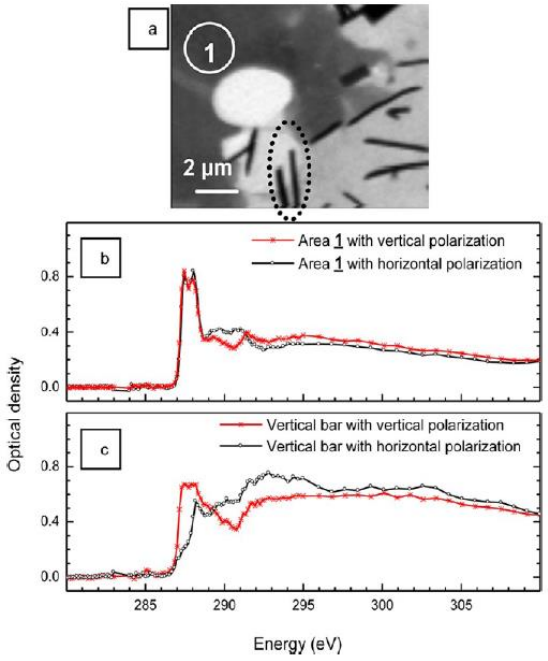

Figure 1-22: STXM image of C36 recorded at 288.2eV (a). The corresponding spectra of the area labelled 1 (b) and the dark vertical bars circled with dashed lines (c) are shown below. Figure reprinted from Masnadi *et al.*[34] with permission.

As shown above, NEXAFS is a powerful technique in determining the orientation of thin *n*-alkane films. When paired with a technique that offers spatial resolution, information about the orientation of specific areas of a film can be obtained. By utilizing *ex situ* PEEM, the intermediate stages of film growth can be observed while obtaining elemental and orientation information from specific domains of a film. The implementation and practical considerations for this technique will be described in section 2.

1.4.4 Unresolved Questions

The previous studies discussed have given important insight into the mechanisms of growth on *n*-alkanes on HOPG (0001), particularly for early stages of growth and for thicker films. The epitaxial growth on *n*-alkanes on HOPG (0001) is an incredibly complex process however, and many factors influence the growth of *n*-alkane thin films such as substrate, temperature, film thickness, deposition rate, surface type, and the symmetry of the substrate. As more of these kinetic and thermodynamic parameters are studied, more questions are sure to arise. Of particular interest is the mid stages of growth, where interactions with the substrate become weaker and morphologies of the deposited *n*-alkanes begin to change.

Previous research[31, 34] has suggested a Stranski-Krastanov growth mode for the epitaxial growth of *n*-alkanes on graphite (see *Figure 1-19*(b)), where the initial stages of growth cover the entire substrate surface with *n*-alkane, followed by island growth after one or more monolayers are deposited (see Figure 1-11). It is important to understand the conditions where this change in growth mode occurs in order to be able to engineer films of a controlled morphology. This project will attempt to address the question of intermediate growth conditions and what the effect is on the morphologies of *n*-alkane films.

1.5 Research Objectives and Approach

The object of the project is to study the intermediate stages of *n*-alkane growth on highly ordered graphite. An *in situ* approach, where the film is observed while it grows, is ideal for this research, and has

been used in previous studies to observe the growth of *n*-alkane thin films[16]. This is not practical in this case however, due to the sensitivity of the materials being observed and the limitations of the instrument being used. It is impractical to evaporate *n*-alkanes in the PEEM main chamber because the *n*-alkane will adsorb to the optical components, contaminating the microscope as discussed below. To address this, an *ex situ* approach will be developed and utilised which has many of the advantages of an *in situ* technique, but avoids the problem of contamination of the PEEM.

The PEEM technique has been used with great success as an *in situ* approach to absorption studies such as metal catalysis of gasses[25, 38]. The majority of these studies are on ideal systems however, such as the absorption of gasses, where contamination of internal components and vacuum degradation are not an issue. Alkanes present a particular difficulty where advantageous build up or the evaporated compound will quickly spoil the cleanliness of the ultra-high vacuum environment of the instrument. Removing this contamination is costly and time consuming, and even a high temperature bake out of the instrument may not be able to remove the contamination, rendering an *in situ* study of alkanes with PEEM impractical.

In order for the *ex situ* method to be utilized, a custom evaporator must be built and attached directly to the PEEM (section 2.2). To prepare *n*-alkane films, the evaporator must be able to sublime small amounts of powdered *n*-alkane onto a substrate that has been heated to a stable temperature. This requires a stable method of heating the sample (section 2.3.2), as well as a method to monitor the rate of *n*-alkane absorption to the sample surface (section 2.3.4).

To study the early to mid-stage growth of *n*-alkanes on highly ordered graphite, a method needs to be developed that addresses many of the challenges that are inherent to *n*-alkanes and their growth on graphite. The largest of these challenges relate to the sensitivity of these materials to damage from high energy light, as well as the quality of the grown films. This work will attempt to develop methods to study

the early to mid-stage growth of *n*-alkanes on HOPG by minimizes sample damage from high energy light that allows these films to be studied while they grow.

Chapter 2 – Experimental Methods

The ideal method to study the early to mid-stage growth of alkanes on graphite would be to observe the growth of the film while it is happening, called an *in situ* measurement. This method is unsuitable for use in the PEEM however as the alkane would coat the interior of the microscope main chamber during sublimation, leading to degradation of the UHV environment and contamination of the optical elements of the microscope. In order to avoid these issues, an *ex situ* process has been developed. The *ex situ* method involves depositing the sample in a preparation chamber attached adjacent to the PEEM main chamber and transferring it to the PEEM without exposing the sample to the atmosphere. This method allows samples to be prepared on site, without exposing them to ambient pressures before analysis. While this method does not allow samples to be studied during growth, it enables the opportunity for successive depositions without compromising the cleanliness of the PEEM optics or the integrity of the of the UHV environment of the microscope main chamber.

2.1 Constraints

This *ex situ* approach to deposition of *n*-alkanes presents a design challenge, as suitable space at the Canadian Photoelectron Emission Research Spectromicroscope (CaPeRS) PEEM end station of the Spectromicroscopy SM beamline is limited due to the large amount of beamline optics, as well as UHV pumps, electronics, and power sources. As a result, free space is scarce and any additions to the end station need to be made as compact as possible in order to fit in the limited space available. In order to accurately model the additions to the CaPeRS PEEM to make sure space requirements are adhered to, extensive use of the 3D drafting software AutoCAD^{TM} was used. The program allows 3D models to be made that accurately represent the real structures. Structures are modelled in pieces with accurate

dimensions and put together to form the proposed structure. In this way, designs can be drafted and measured to determine suitability for the space requirements, as well as aid in manufacturing.

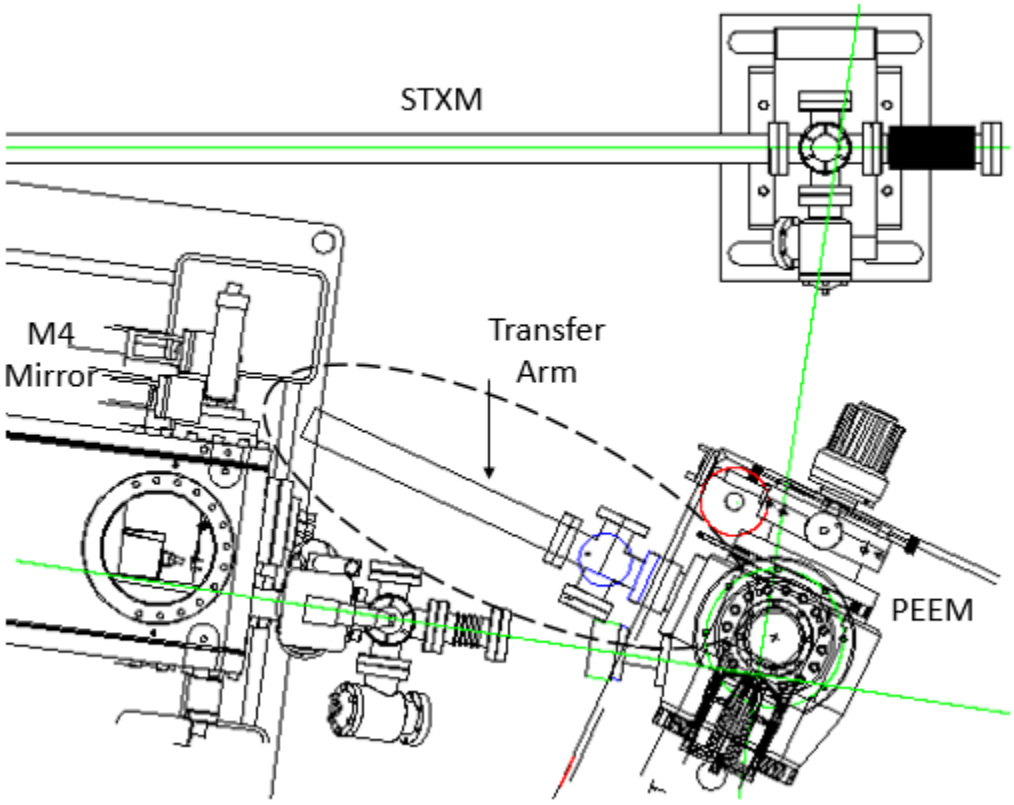

Figure 2-1: Schematic of the PEEM microscope sample loading area at the SM beamline. The dashed circle indicates the area where the ex situ evaporator must be placed. ACAD file credit to Elmitec GmbH and the Canadian Light Source.

Figure 2-1 shows an overhead view of the CaPeRS sample loading area at the SM beamline. The area where the *ex situ* evaporator was installed and the transfer arm is circled with a dashed line. The area sits between a mirror (M4 PEEM) (left) and the microscope main chamber (bottom right). The total length of the transfer arm and the load lock chamber, which must be shorter than the distance between the main chamber and the M4 PEEM mirror, is a distance of 520 mm.

The current load lock chamber for the microscope is a custom manufactured five-way cross with two ports offset at angles greater than 90 degrees to facilitate sample loading and observation. The *ex situ* project requires a six sided chamber with ports angled 90 degrees from each other however, so using the

current chamber is impossible. The six ports are required for mounting the quartz crystal balance (QCB) (see section 2.3) (above), evaporator and pump (below), transfer arm, heating stage, PEEM main chamber, and observation window (sides). These must be angled at 90 degrees relative to each other to facilitate the advancement and retraction of the transfer arm and heating stage, as well as maintaining the evaporator and QCB directly below and above the sample, respectively. Using a standard six-way cross is not possible, as the total length of the cross is 125 mm. When paired with the transfer arm, gives a total length of 525 mm, which is larger than the space available, as shown in Figure 2-1. However, six-sided cubes are available with tapped holes for mounting CF flanges with a total length of only 70 mm. One of these cubes, with a rotatable close coupler mounted, will be used for the main chamber of the *ex situ* evaporator.

2.2 Evaporator Preparation Chamber

In order to maximize the usability of the available space, the main chamber of the evaporator is designed around a commercially available cube. The cube is a single piece stainless steel construction with areas to mate with Conflat™ [*] (denoted CF herein) flanges on all six sides and tapped bolt holes. This gives the smallest available way to mount 6 flanges to a central chamber, without resorting to custom-manufactured products. The main chamber of the microscope also has tapped bolt holes for mounting a CF flange. These bolt holes are rotated approximately 40 degrees from center, which necessitates a rotatable coupling flange able to utilise the tapped holes. The part used is a specialty flange obtained from Kimball physics, as shown in Figure 2-2. This piece allows two flanges with tapped bolt holes to be mated with minimal length added, only 35.5 mm in this case.

[*] ConFlat is a trademark of Agilent Technologies

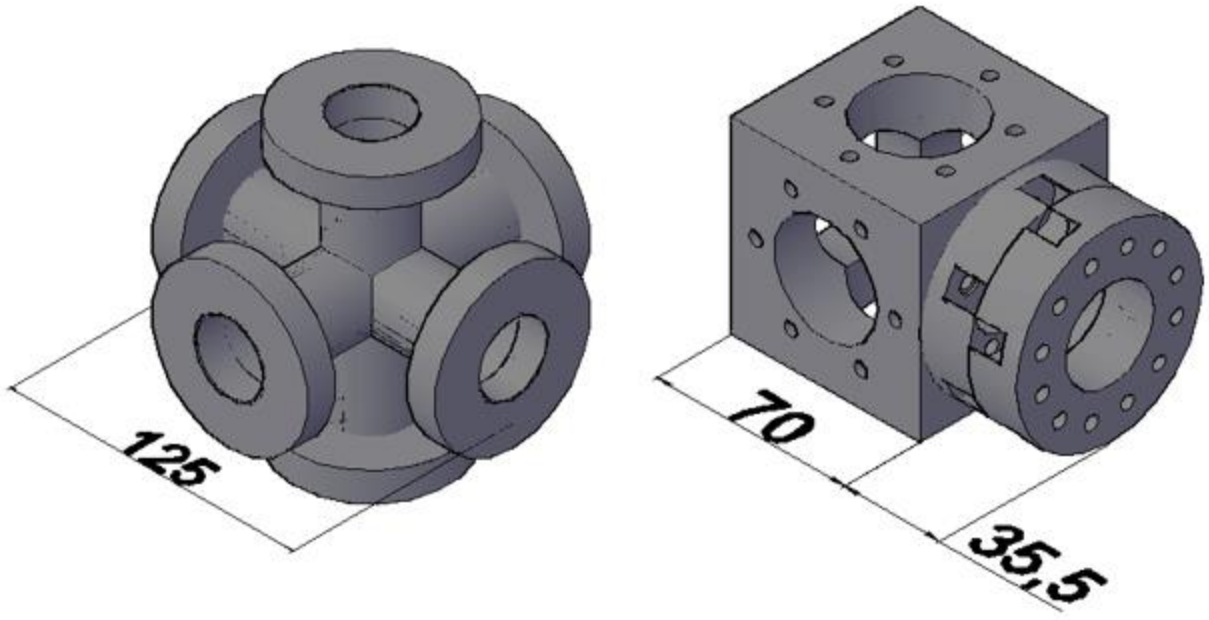

Figure 2-2: Models of a standard 6-way cross (left) and a 6-way cube with a rotatable lose coupler attached (right).

While the standard 6-way cross allows rotatable mounting without additional hardware, the total length of the 6-way cross is 125 mm. While this is only 19.5 mm shorter than the cube with rotatable close coupler attached, it is nevertheless a significant enough amount to make the 6-way cross unusable in the confines of the available space.

Figure 2-3 shows a three-dimensional CAD schematic of the design for the *ex situ* evaporator. The heating stage, QCB, and evaporator can be seen mounted to the evaporator main chamber in their respective positions. The rotatable close couple is attached to the CF flange of the cube in the direction positive z-axis, while the transfer arm will be mounted to the flange at the negative z-axis position. An image of the functioning evaporator installed on the laboratory bell jar is shown in Figure 2-4. This same setup is used at the SM beamline with the exception of the PEEM main chamber at the position that the bell jar is in.

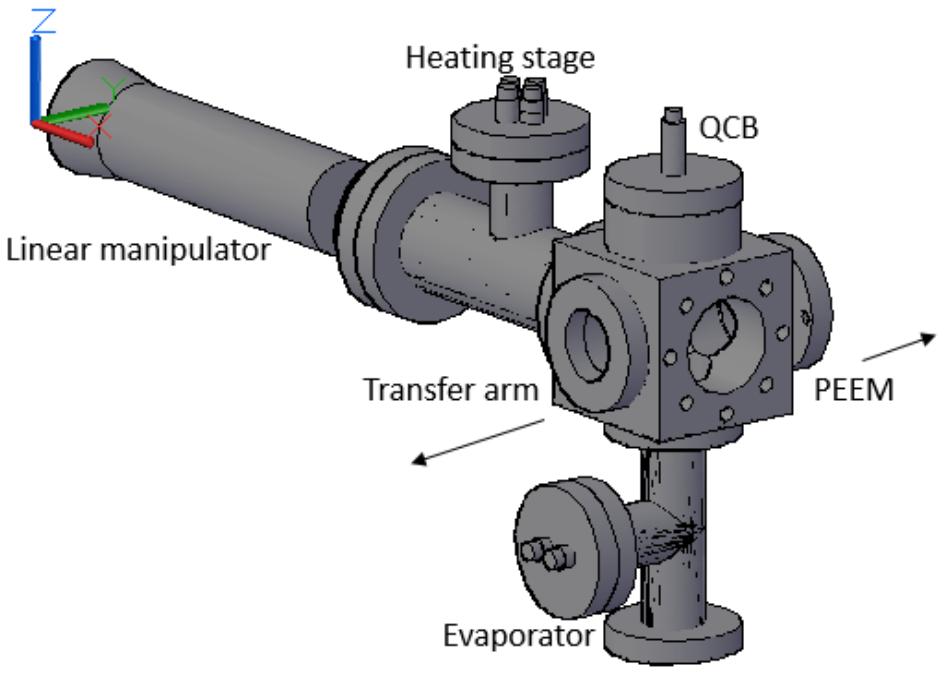

Figure 2-3: Schematic of the design for the ex situ evaporator. The transfer arm and microscope main chamber are attached to the evaporator chamber on the positive and negative y-axis, respectively.

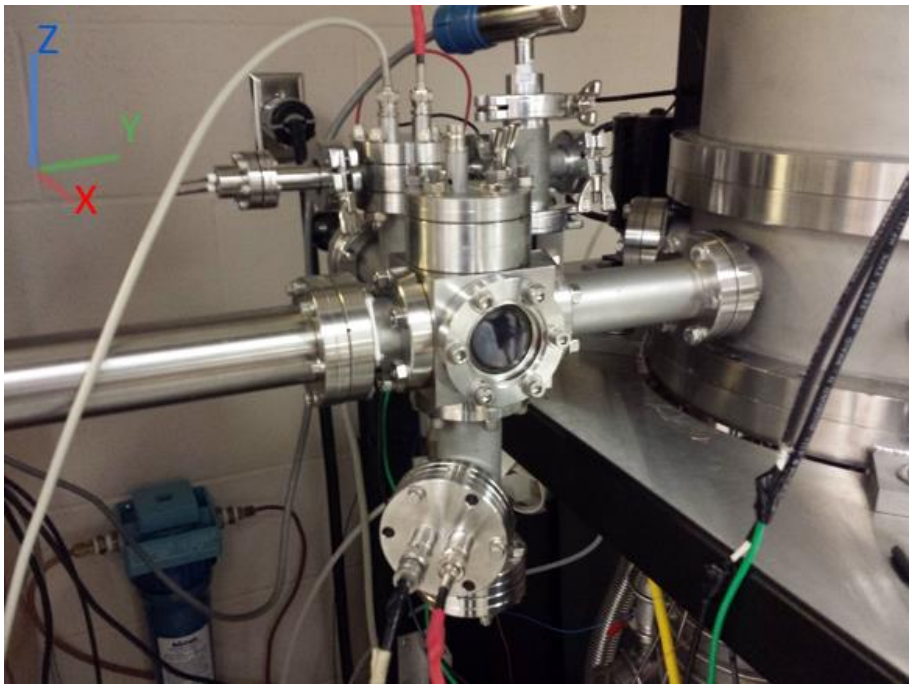

Figure 2-4: Image of the ex situ evaporator connected to the bell jar in the on campus lab. The laboratory bell jar was used for preliminary testing. Axes are the same as in Figure 2-3.

In order for the sample to be transferred from the evaporator chamber to the PEEM main chamber, the evaporator chamber needs to have vacuum conditions near to the UHV conditions of the main chamber. In addition, the pumping system must be quick and versatile, capable of quickly pumping form atmospheric conditions when the sample is first inserted. To accomplish this, a small turbomolecular pump is used with a mechanical roughing pump. The turbomolecular pump is mounted directly below the evaporator. The turbomolecular pump is capable of reducing the pressure of the evaporator chamber to less than 10^{-7} Torr, which allows the main chamber to be opened and the sample transferred. The vacuum conditions are monitored by two gauges: a Pirani gauge for low vacuum (down to 10^{-3} Torr), and an ion gauge for high vacuum down to 10^{-10} torr. In addition to the low vacuum pressure, the Pirani gauge allows for easy identification of leaks in the system. The ion gauge is used to monitor high vacuum conditions, as it cannot be used at pressures above 10^{-3} Torr.

By using the design outlined in the previous figures, the *ex situ* evaporator can be made to fit in the confined space available at the CaPeRS PEEM end station. A large amount of design has been undertaken on the internals of the *ex situ* evaporator in order to conform to the restrictions of the above design. Below the design of the internal components of the *ex situ* evaporator will be discussed.

2.3 Internal Components

In order to grow films by the *ex situ* method, the custom evaporator needs to include several necessary functionalities, while adhering to strict space restrictions. The *ex situ* evaporator requires a sample heating stage to maintain the proper temperature of the substrate, a crucible that holds the alkane sample to be evaporated, and a QCB to monitor the rate of deposition. A custom short transfer arm tip will also be designed and manufactured to reduce the overall length of the transfer arm. The design, manufacture, and implementation of these components will be discussed below.

2.3.1 Transfer Arm Tip

The area with the greatest space restriction is along the axis of the sample transfer arm, and the transfer arm of the CaPeRS PEEM had been previously designed to a shorter length than a standard transfer arm as ordered from a manufacturer. The transfer arm tip is attached to the in-vacuum end of the transfer arm and allows the sample to be transferred from the load lock into the PEEM main chamber without having to vent the microscope main chamber. The transfer arm tip utilized a spring and pin mechanism to secure the sample holder in place until it is transferred to the main chamber. The tip that was already mounted to the transfer arm was not designed to minimize the overall length. As a result, the current transfer arm tip cannot be used without interfering with the motion of the *ex situ* evaporator heating stage. In order to use the current transfer arm and avoid have a completely new transfer arm designed and built, a new tip to hold the sample holder was designed and fabricated. The new design, seen in Figure 2-5 and Figure 2-6, has a total overall length of 19.5 mm. This is 23.5 mm shorter than the current transfer arm tip. The new tip was manufactured from copper and stainless steel by the Physics Machine Shop on the University of Saskatchewan campus. The shorter transfer arm tip is necessitated by the smaller overall length of the 6-way cube, compared to the 6-way cross.

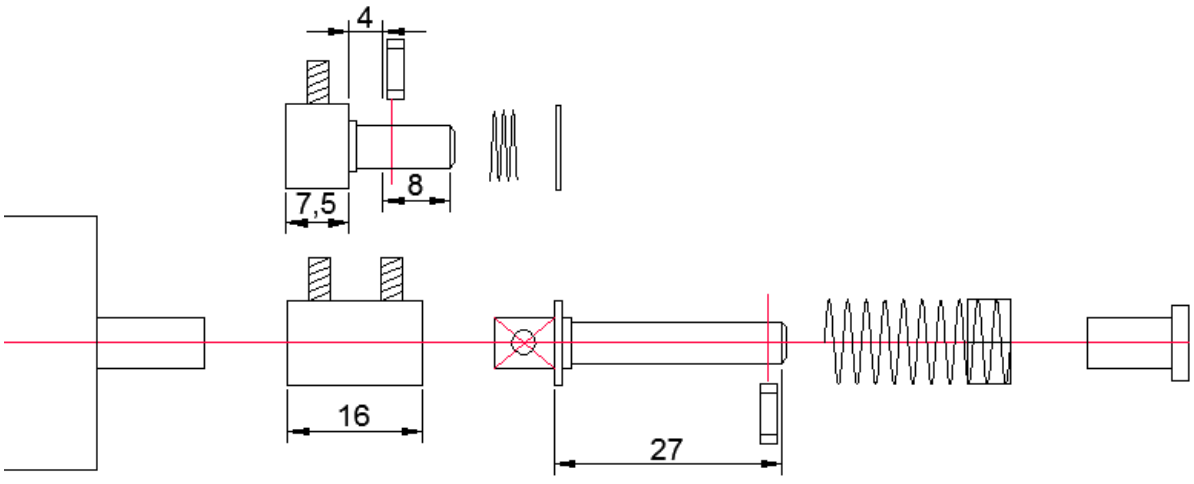

Figure 2-5: Schematic of the redesigned transfer arm tip (top) and the original transfer arm tip (bottom). The total lengths for the redesigned and original tips are 19.5 mm and 43 mm, respectively.

Figure 2-6: Redesigned transfer arm tip (left) and original tip (right). They are seen attached to the transfer arm.

The redesigned tip is attached to the transfer arm with a set screw that turns into a recess in the bottom of the tip. The sample holder is secured to the transfer arm by a pin that rotates into the bottom of the sample holder. A spring ensures that the sample holder remains secured during use. The sample holder can only be removed by applying pressure and rotating the transfer arm. The newly designed transfer arm tip allows the sample holder to be manipulated in the same manner as before, but with a reduced length profile. This smaller length is required for transferring samples to the heating stage described below.

2.3.2 Heating Stage

In order to control the morphologies of the deposited alkanes, it is necessary to control the temperature of the substrate during deposition. The CaPeRS sample holder is equipped with a tungsten heating filament that allows the sample to be heated up to 600 ^{0}C with resistive heating, and up to 1500 ^{0}C with electron bombardment. The sample holder also has a C type (W/Re 95%/5% – W/Re 74%/26%, by weight) thermocouple in order measure the sample temperature. The heating filament and thermocouple of the sample holder is designed to function in the vacuum of the PEEM main chamber. In order to control the temperature during sample preparation, a heating stage needed to be created that would fit in the confines of the 38 mm evaporator chamber diameter while utilizing the heating filament and thermocouple of the CaPeRS sample holder. The heating stage was manufactured from copper because copper is easily machineable and has favourable thermal properties. Machining work was performed at the Physics Machine Shop.

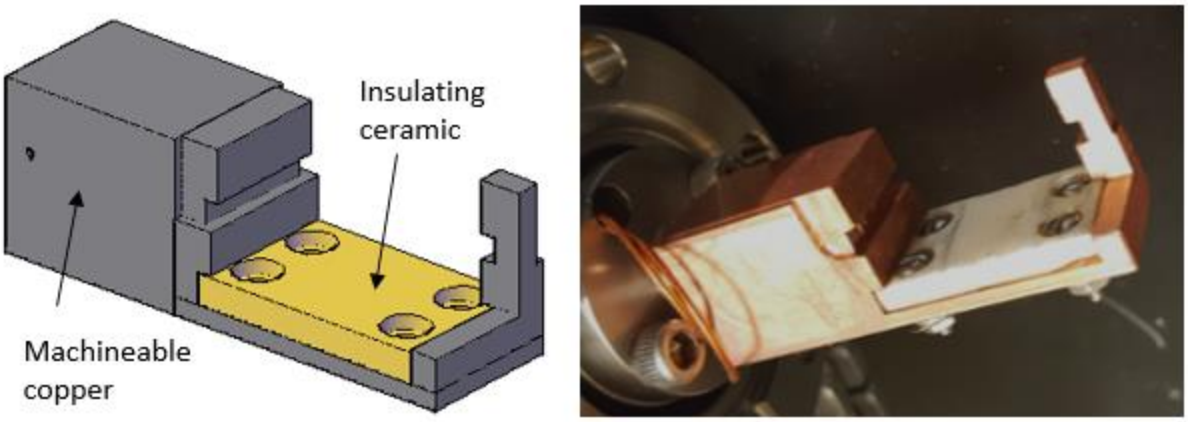

Figure 2-7: (left) 3D CAD drawing of the sample heating stage that has been designed. The main piece is made from machineable copper. The yellow plate is made from machineable ceramic and insulates the heater and thermocouple connections from the frame. This piece was manufactured by the Physics Machine Shop (right). The finished heating stage, connected to the linear manipulator.

The heating stage is shown in Figure 2-7. The stage features four stainless steel contact pins, insulated with ceramics, attached to wires for the sample heating filament and the thermocouple. These are attached to feedthroughs on a stainless steel three-way cross. The heating stage is mounted on a linear manipulator to allow it to be advanced and retracted from the evaporator. The sample holder is mounted so that the surface of the sample points downward, towards the evaporator. Note the mounting area for the sample holder is cut out on the front side to allow the heating stage to be retracted when the sample is on the transfer arm.

The heating stage allows the desired temperature of the sample to be maintained, as is required for the epitaxial growth of *n*-alkanes using PVD. The design and function of the evaporator be discussed below.

2.3.3 Evaporator

The evaporator consists of a ceramic crucible to hold the alkane, with a tungsten wire coiled around it to create a filament that provides heat when current is applied. The crucible is held in place by the tension of the tungsten wire with no additional support needed. The filament is connected to feedthroughs and a power source is connected to provide current, typically around 1.5 amps, 1.0 volts for

C36. While this filament is not able to attain the high temperatures needed for the evaporation of metals, it allows temperatures suitable to evaporate organics. Both the heating stage and the evaporator are controlled by a dual output power supple capable of 0-30 DC volts and up to 5 A.

During initial evaporations, it proved difficult to control the rate of evaporation effectively, as temperature of the evaporator fluctuated considerably as the mass of the *n*-alkane was reduced through sublimation. To solve this, a platinum resistance temperature detector (RTD) was attached to the ceramic crucible with low vapour pressure epoxy. The resistance of the RTD will increase linearly as temperature increases, and by monitoring the resistance of the RTD the temperature of the crucible can be kept constant. The relationship between resistance and temperature for this particular RTD is given by the equation below:

$$R(\Omega) = 3.85 * T(^0C) + 1000 \quad \text{(2.1)}$$

where R is the resistance and T is the temperature. Using a multi-meter to monitor the resistance of the RTD allowed quick and accurate measurement of the crucible temperature, allowing the evaporation rate to be kept constant.

2.3.4 Quartz Crystal Balance

The rate of deposition and final thickness of the adsorbed material is measured with the use of a quartz crystal balance (QCB). QCB thickness monitors operate on the principle of the piezoelectric effect, where a crystal experiences a deformation when a voltage is applied. When an alternating voltage is applied to a quartz crystal, a common type of piezoelectric crystal, a standing wave is generated at a resonant frequency. This resonant oscillation has a very narrow resonance that is highly stable, allowing the frequency to be determined with high accuracy.

As material is adsorbed, the oscillation of the crystal is dampened. This dampening is directly proportional to the amount of adsorbed material, and if the density of the adsorbate is known, the total thickness and deposition rate can be calculated with high accuracy.

The evaporation rate was measured with a quartz crystal micro balance. The QCB was mechanically attached to a CF flange with a single feedthrough for the QCB. This was attached to the top of the cube to measure the rate of deposition. The QCB was controlled with a Sigma SQM 160 rate/thickness controller, which allows accuracy in rate determination to 0.1 Å/s and thickness of 1 Å. Since the QCB is obstructed by the sample during the deposition, the final thickness of the prepared film is calculated by multiplying the rate of deposition by the time taken. The rate is measured before and after the deposition, and the temperature of the ceramic crucible is kept constant during the preparation to ensure that the rate is constant.

2.4 Deposition Method

Due to space constraints and the geometry of the *ex situ* evaporator, the deposition rate cannot be monitored simultaneously with deposition, as the QCB is blocked when the sample is in the evaporation chamber. To accurately determine the rate and thickness of the sample, the rate is monitored and adjusted while the sample is retracted. When a stable deposition rate is achieved, the sample is advanced into the chamber for a set amount of time to achieve the desired thickness. After deposition, the sample can then be retracted once more and the rate measured to ensure that it remained constant for the entire deposition.

The deposition rate that is measured at the QCB will be less than the rate at the surface of the sample. This is because the sample is closer to the evaporator than the QCB is. The surface of the sample is 97.5 mm from the evaporator crucible, while the surface of the QCB crystal is a distance of 117.5 mm from the crucible. This means that the deposition rate at the sample will be approximately 69% larger than at the QCB.

2.5 Materials and Methods

There are many different *n*-alkanes that can be used to create ordered films by PVD based on their varying chain lengths[34]. There are different options for graphitic substrates that can be used to grow ordered thin *n*-alkane films as well. The *n*-alkanes used for this work were selected based on their vacuum

compatibility and the reproducibility of *n*-alkane morphologies created, while the graphitic substrate was selected for its ability to be characterized before deposition. The sections below detail what materials are used to create the samples, as well as the methods used to characterize the films and substrates, both before and after sample preparation.

2.5.1 *n*-alkanes Studied

The *n*-alkane chosen the majority of depositions was hexatriacontane ($C_{36}H_{74}$; C36). As the length of the *n*-alkane increases, the temperature required to sublime the *n*-alkane increases as well. In order to keep similar morphologies at these increasing chain lengths, a higher substrate temperature is needed for the vapours to deposit on in order to get similar morphologies[39]. C36 was chosen due to the moderate substrate temperature (approximately 46 ^{0}C) needed to obtain a morphology with well-ordered domains (see Figure 1-19), as well as its relatively high vapour pressure when compared to other alkanes. It was also determined experimentally that C36 was the *n*-alkane that gave the most reproducible patterns, which was consistent with the literature[34].

2.5.2 Substrate

There are several types of graphite that can be used to grow alkane films on, including highly ordered pyrolytic graphite (HOPG) and graphene grown by chemical vapour deposition[34]. As the substrate is carbon, the substrate can contribute to the NEXAFS spectrum that is measured. This is especially problematic for thin films, where there can be significant spectroscopic contribution from the substrate. The contribution to the spectrum from the graphite substrate can be minimized by using a sufficiently thin graphite layer as the substrate.

For this research, Kish graphite applied to a silicon, or silicon dioxide substrate was chosen. Kish graphite is high-quality graphite flakes produced as a byproduct of steel making. Thin flakes of graphite on SiO_2 was prepared by the mechanical cleavage method[40]. This yields a surface that is covered in graphite pieces of various sizes ranging from several layers down to one mono layer (graphene). The

adhesive residue from the tape is removed by washing on a 1:1:1 mixture of acetone:toluene:methanol for 30 mins. The resulting clean, bare support surface provides an area with which to take a reference spectrum for normalization during analysis. To ensure minimal contribution to the spectrum from the underlying substrate, graphene or few layer graphene areas were measured.

2.5.3 Support for Substrate

The PEEM technique requires that samples be conductive. For this reason, p-doped silicon is used as a support for the graphite. The silicon support allows charge to be carried through the sample to neutralize the charged surfaces. Silicon and helps aid in the identification of thin graphite and graphene flakes on the surface. Large graphite flakes are visible to the unaided eye, and smaller flakes are easily observed with the use of optical microscopy. Thin graphite flakes that are ten layers thick or less are not able to be distinguished from their thick counterparts on pure silicon however, with optical or electron microscopes. For this reason, silicon with a 90 nm layer of oxide is used as the support for the substrate. Silicon wafers with a thin oxide layer allow easy identification of graphene by optical microscope with illumination with visible light. Graphite composed of ten layers or less appears darker in colour than thicker flakes when viewed under optical microscopes. The thin flakes are sufficiently transparent to visible light and add to the optical path of the light. This changes their interference color when compared to the bare SiO_2 surface[41].

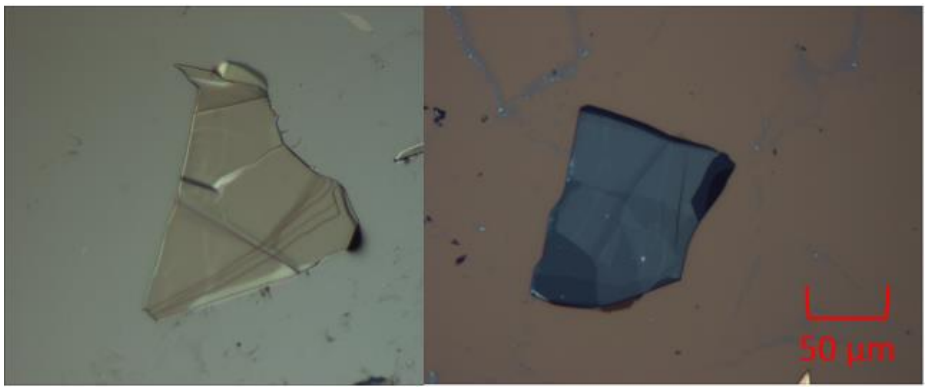

Figure 2-8: A comparison between similar graphite flakes on bare silicon (left, 50X objective) and on silicon dioxide (right, 50X objective).

As shown in Figure 2-8, it can be clearly seen that graphite has greater contrast with the substrate when on 90 nm silicon dioxide (right) compared to bare silicon (left). Different thicknesses of the graphene layers can be discerned by their relative contrast to the other layers, with thin layers appearing darker and thick layers lighter. These effects are not visible when on bare silicon. Optical microscopy will be used to characterize the substrate surface before thin film growth.

The insulating oxide layer of the silicon dioxide support was thought to have presented a problem for use with the PEEM by allowing charge to build up in the sample. When the number or electrons entering the system is greater than the number leaving, a positive charge is built up on the surface of the insulator until an equilibrium is reached[17]. This phenomenon is called charging and leads to a range of problematic effects (see section 1.2). Charging causes abnormal contrast changes, image deformation and shifts in the image. Sudden releases of electrons will cause bright flashes on the screen, potentially causing damage to the multi-channel plate and tripping the high voltage interlock of the instrument (see section 1.2). It was experimentally determined that 90 nm oxide was suitable for use in the PEEM when the intensity of the X-ray beam is reduced (see section 3.3.3).

2.5.4 Characterization Methods

After graphite has been transferred to the silicon support and cleaned (see section 2.5.2), the substrate is viewed under an optical microscope to ensure that the surface is sufficiently covered with graphite. Optical microscopy can also be used to identify single layer graphene flakes and verify the cleanliness of the substrate. Optical microscopy can also be used to view deposited alkanes. Figure 2-9 shows the patterns formed by C36 on graphene and graphite flakes when evaporated onto the substrate at 41 °C. Patterns of small ordered bars cover the surface of the substrate. The patterns can be seen on several graphite pieces and show no variation with thickness of the graphite flakes.

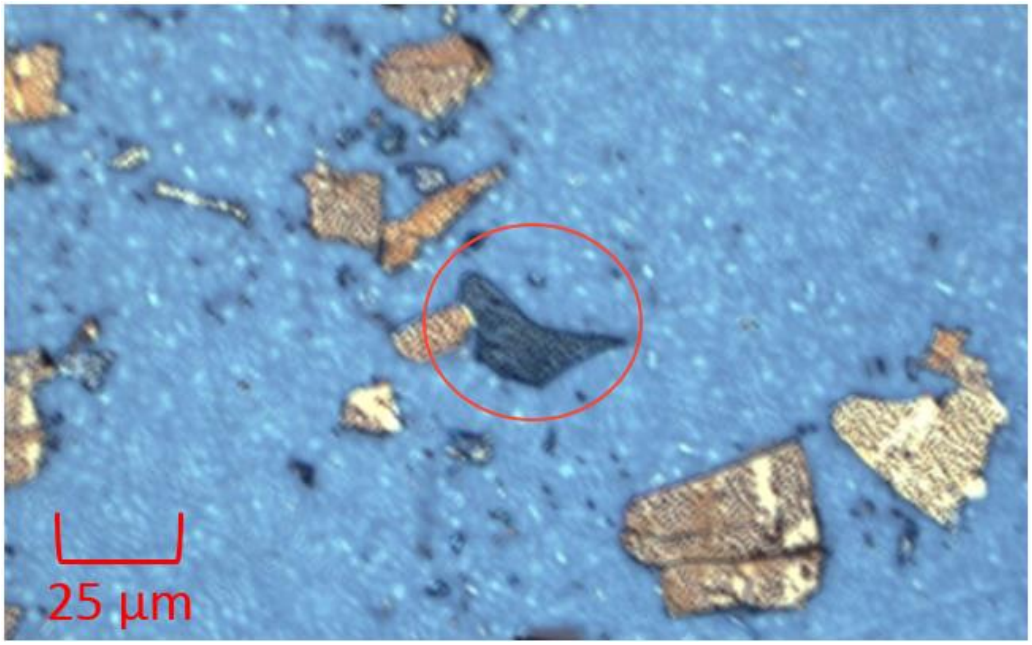

Figure 2-9: Patterns of 70nm thick of C36 deposited on graphite and graphene flakes (25X objective). The patterns formed by the alkanes are identical when formed on graphite or graphene (circled in red). Sample prepared in on laboratory thermal evaporator jar.

Before the sample is deposited, the bare substrate is viewed in the PEEM with UV illumination from the Hg arc lamp. The UV source is polychromatic and low intensity; NEXAFS spectra cannot be obtained with the Hg arc lamp. However, UV light provides better spatial resolution that X-rays. This arises from the lower energy of UV light creating photoelectrons with a narrower range of energies, leading to less chromatic aberration. The Hg arc lamp illuminates the entire sample, which allows for easier focusing and tilt adjustments of the sample. *n*-alkanes are sensitive to UV light and undergo photolysis under UV light. Since the UV source illuminates the entire *n*-alkane sample, it causes the entire surface to become damaged. Therefore, UV light is not useful for studying prepared films. UV light is used to focus and find acceptable graphite flakes to study on the substrate before the deposition.

Graphene is very difficult to identify under UV illumination however, so higher thickness flakes are used as land marks to find areas with graphene. Figure 2-10 shows a Si/SiO_2 support with graphite and graphene areas adhered. The dark flake in the center of the image that is circled in red shows a graphene flake. It can be seen that graphene is easily identified in the optical microscope image, but very

difficult to see graphite thinner than 10 layers under UV light in the PEEM (left). Final characterization of the sample is done with synchrotron light from 270 eV to 310 eV (right). The graphene area is clearly visible under X-ray illumination but cannot be distinguished from the thicker graphite flakes. A combination of optical microscopy and UV illumination in the PEEM allows suitable flakes to be identified before sample preparation.

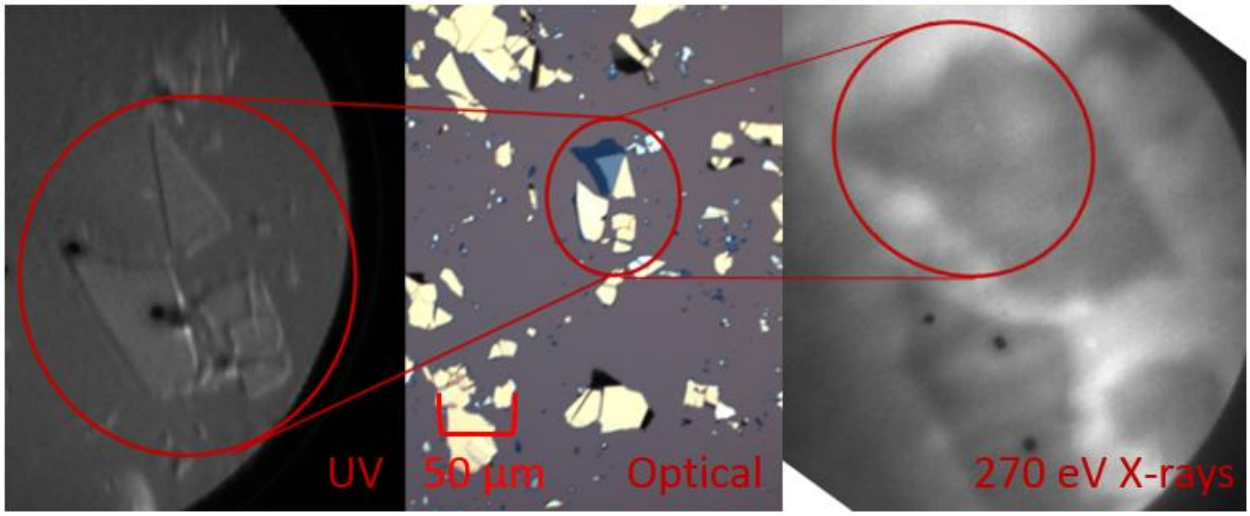

Figure 2-10: Sample surface before evaporation. The images show the sample illuminated with UV light in the PEEM (left, 200µm FOV), optical microscope (center, 50X objective), and 270 eV X-ray radiation (right, 50µm FOV). The same area is circled in each image.

-The poor quality of the X-ray PEEM image (right) when compared to the UV PEEM image (left) should be noted. The blurry image and poor focus are due in part to greater chromatic aberration from the X-ray electrons, as well to charging from the SiO_2 sample support. These issues will be addressed in the following chapter by reducing the intensity of the X-ray beam, which is at full power in the figure above.

Chapter 3 – Results

3.1 Alkane growth on HOPG

The molecular orientation of alkanes deposited on graphite is highly dependent on the deposition conditions, such as substrate temperature and deposition rate. For this project, the laboratory thermal evaporator in a high vacuum bell jar was first used to study the proper deposition conditions and to make samples to test the viability of PEEM measurements. Optical microscopy is also used to study samples before PEEM measurements are taken to characterize the growth patterns. Herein will be presented the characterization of samples prepared with the laboratory thermal evaporator and samples prepared with the *ex situ* evaporator. Comparisons will also be made between the two methods of sample preparation.

3.1.1 Laboratory Results and Characterization

Previous Urquhart group studies[7, 34, 39, 42] have developed well-defined procedures to deposit *n*-alkanes on HOPG substrates. Graphite and graphene flakes adhered to a silicon support had not been extensively studied as a substrate however, and initial work was focused on using the on laboratory thermal evaporator to develop a procedure to consistently create the desired morphologies of *n*-alkanes on the graphite substrate. The properties of the substrate, such as heat capacity and thermal conductivity, will vary between differing thicknesses of graphite. This will lead to different morphologies being observed, even when the deposition conditions, such as substrate temperature and deposition rate, are identical [7, 34]. It is therefore important to develop a procedure that gives reproducible results for the substrate being studied. Figure 3-1 shows a C36 film deposited on graphite flakes supported on Si/SiO_2 under an optical microscope (left) and in the PEEM (right). The deposition conditions that gave these and similar results were a substrate temperature of 46^0C, while depositing at a rate of 0.5-1.0Å/second. The patterns of bars were not as wide and pronounced as there are on HOPG squares, as shown in section 1.4.2. The variance

in morphologies is related to the differences in substrate properties; while the solid HOPG substrate is uniform, graphite on silicon has discrete domains with varying thickness. These differences may cause slightly different morphologies to be observed, even when the deposition conditions are identical. The small domains showed a six-fold symmetry and were able to be reliably produced.

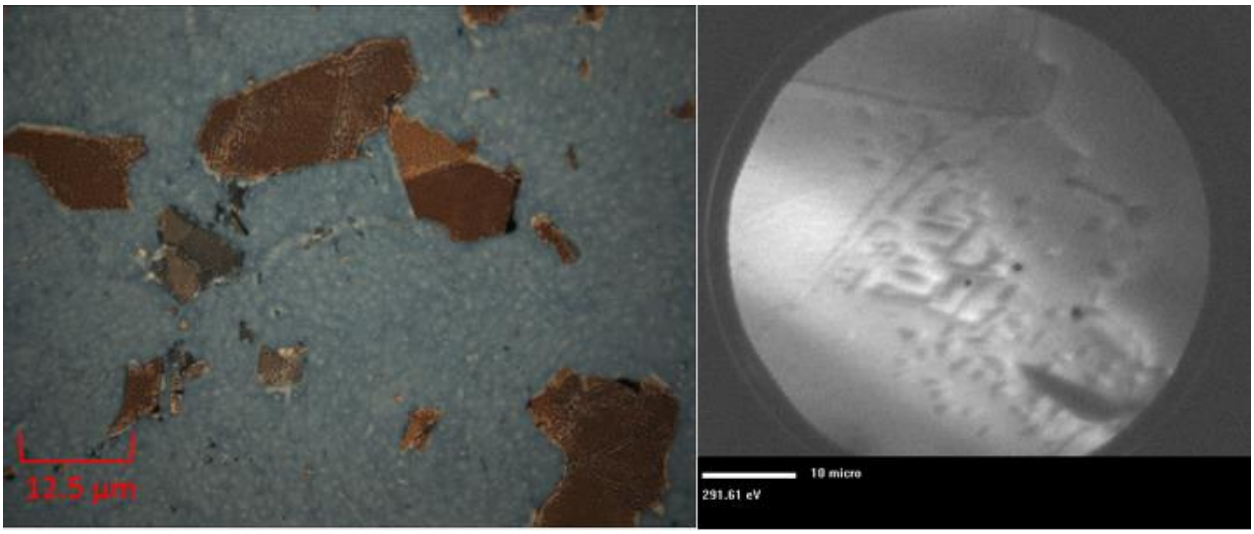

Figure 3-1: C36 on graphite (left, 100X objective), prepared with the laboratory thermal evaporator. The temperature of the substrate was maintained at 46^0C throughout the deposition. The final thickness of the sample is 50 nm. PEEM image of C36 on graphite (right, 50µm FOV). Sample was prepared with the laboratory thermal evaporator.

Samples created with the laboratory thermal evaporator were also studied using PEEM (Figure 3-1 right) to examine the effects of radiation damage, as well as to determine the optimal experimental parameters to collect NEXAFS spectra. Samples prepared on campus for use at the CLS were sealed in a plastic bag filled with nitrogen gas to avoid air exposure during transportation to the SM beamline. Prepared samples were also stored in darkness during transportation to avoid UV induced photolysis.

3.1.2 *Ex situ* Evaporator Results and Characterization

The *ex situ* evaporator functions very similarly to the laboratory thermal evaporator, with the exception that the sample is not exposed to air when transferring to the microscope main chamber. Since the deposition rate cannot be monitored simultaneous with the sample preparation, care was taken to

ensure that the crucible was kept at a constant temperature to maintain a steady rate of alkane sublimation. For more detail on the evaporator, see section 2.3.3.

Before samples are prepared in the *ex situ* evaporator, the bare substrate is first observed in the PEEM. This allows the sample to be focussed and its tilt adjusted before there is alkane deposited on it. Adjustment of the sample tilt in the PEEM is required in order to achieve proper focus of the sample, and must be adjusted separately for each individual sample. If the sample is not perpendicular to the electron axis of the microscope the images will be distorted. Adjusting the tilt prior to alkane deposition also allows the entire substrate surface to be illuminated with UV light, greatly simplifying the tilt adjustment process when compared to the X-ray beam, which only illuminates a small area of the sample surface. The surface of the substrate may also be observed before alkane deposition to find and mark the location of suitable graphite flakes that can be returned to after the alkane deposition is completed. A spectrum of the surface of the clean Si/SiO_2 support can also be acquired here for use in normalization. Figure 3-2 shows a PEEM image of a sample before alkane is deposited. An area with a concentration of large graphite flakes is shown which will be returned to after sample preparation is complete. Completing these steps before the *n*-alkane is deposited on the sample ensures that the sample spends the minimum amount of time in the X-ray beam and will be less damaged by the X-rays compared to a sample where these steps have not been taken.

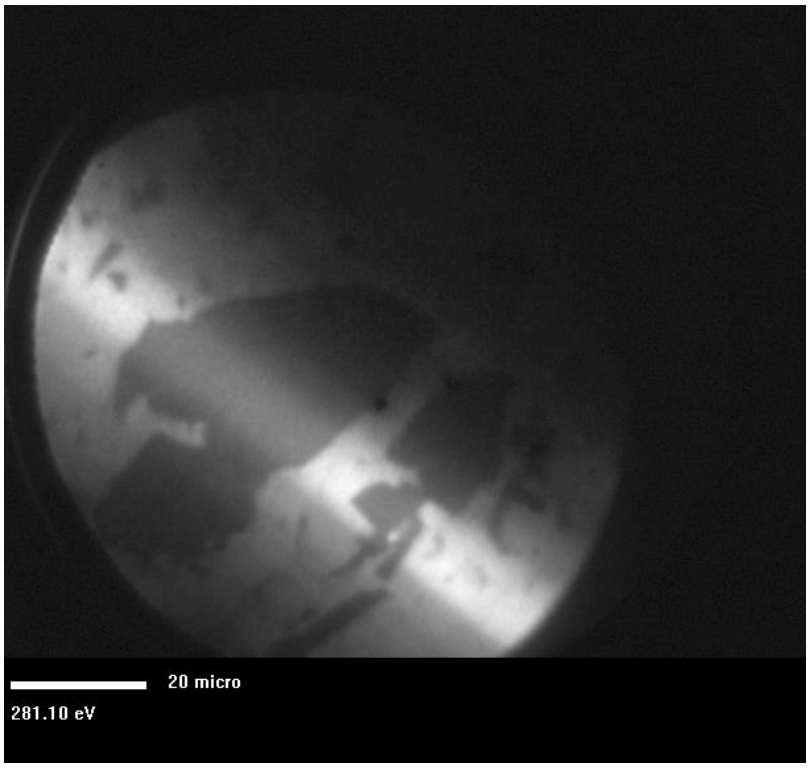

Figure 3-2: PEEM image (100 μm FOV) of the graphite substrate before sample deposition.

Figure 3-3 (left) shows an optical microscope image of a C36 film that was grown in the *ex situ* evaporator. While the alkane domains are not as clear as the ones produced in the laboratory thermal evaporator, thin bars with a six-fold symmetry are observed. Optical microscopy allows the samples prepared in the *ex situ* evaporator to be compared with the ones created with the laboratory thermal evaporator. Figure 3-3 (right) shows a PEEM image of a C36 sample prepared with the *ex situ* evaporator. Many small alkane domains are visible across the surface of the graphite flake. These domains correspond well to the domains produced from the laboratory evaporator.

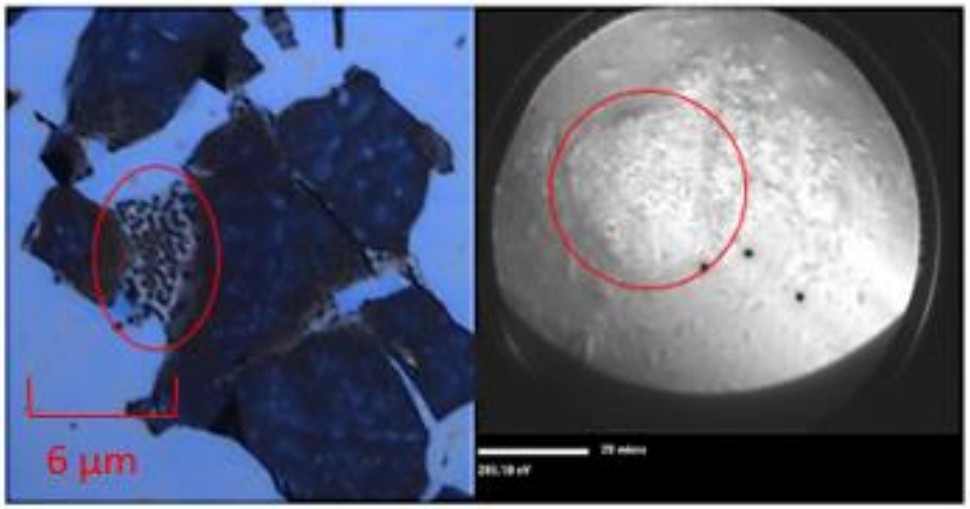

Figure 3-3: Optical image of a C36 film grown in the ex situ evaporator (left, 100X objective). Small domains with six-fold symmetry are present on the graphite and graphene flakes. The areas where the small alkane domains are most visible are circled in both images. The X-ray PEEM image at 285 eV (right, 75µm FOV) of a sample created in the ex situ evaporator. Many small domains are seen on the surface of the graphite flake.

Because the time the sample is under the beam needed to be minimized and the intensity of the X-ray beam needed to be reduced to avoid radiation damage (see section 3.3.1), spectra needed to be collected and averaged from multiple domains in order to obtain data with an acceptable signal-to-noise ratio. Collection of spectra from small domains was also made challenging due the non-uniformity of the X-ray beam (see section 3.3.2). The large number of small domains provides many opportunities to collect spectra from different orientations (see section 3.3.4).

As the results described here show, both the *ex situ* evaporator and the laboratory thermal evaporator gives similar results for the patterns on alkane observed on graphite flakes. The images collected with the PEEM show alkane domains similar to the ones seen in the optical microscope images, and the films grown in the *ex situ* evaporator resemble those produced with the laboratory thermal evaporator. Individual spectra can be extracted from these domains where they can be compared to spectra from alkane domains of different orientations. These results are presented in section 3.3.

3.2 NEXAFS Normalization

NEXAFS spectra are routinely normalized. The normalization process regularizes variations in the light source that arise from the decay of the electrons in the storage ring, contamination of the beamline optics, and other source fluctuations such as changing position of the electron bunches in the storage ring. Normalization can also help to reduce variations that can arise due to amplifier and detector settings. Normalized data can then be compared even when the details of the experiment are changed. The basic procedure to normalize a total electron yield spectrum is to take the ratio of the measured spectrum, termed I, with the incident photon flux, termed I_0. This normalization equation can be written as:

$$I/I_0 \qquad (3.1)$$

At a synchrotron beamline, the intensity for the C 1s edge region of the X-ray beam varies with the energy of the photons, as seen in Figure 3-4. As can be seen in the figure, there are large variation in the intensity of the X-rays that reach the sample as a function of energy. When the sample spectrum is measured, these variations in the X-ray intensity will also be included in the measured spectrum. The normalization process is particularly important when studying carbon 1s spectra as there are large variations in the intensity of incident X-rays over the NEXAFS energy range. The most prominent of these variations occur at 284 and 291 eV and are referred to as the carbon dip. The carbon dip is clearly visible in the spectrum shown in Figure 3-4, and can account for an X-ray intensity drop of over 90%. These carbon dips are the result of carbon impurities deposited on the optical elements of the beamline. Care must be taken to properly normalize spectra as small variations in the in the spectra used to normalize data can result is large changes to the final spectra, particularly at the low intensity regions of the carbon dip. In the following sections, challenges associated with normalization of C 1s spectra will be discussed, and techniques to address these difficulties will be explored.

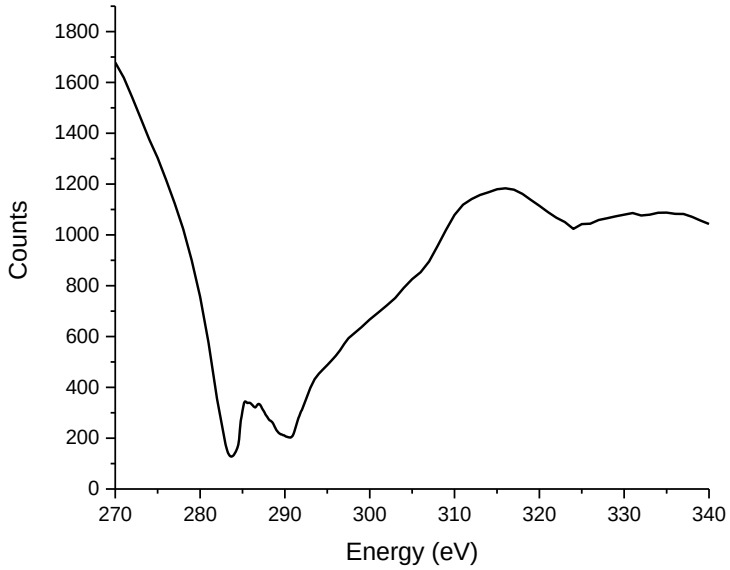

Figure 3-4: Intensity of X-ray beam as a function of photon energy over the carbon 1s edge at the PEEM endstation of the SM beamline.

3.2.1 Challenges for Normalization of *n*-alkane Films

The most crucial step when normalizing a NEXAFS spectrum is to obtain a quality spectrum of the incident photon flux (I_0). The I_0 can be obtained in several different ways, but all require a spectrum of a reference material that does not show any features over the energy range being used for the sample. Targets typically used for I_0 measurements are a gold mesh, nickel mesh, or a silicon photodiode. There are several methods to collect the I_0, however the best results are obtained when the I and I_0 are obtained at the same time, ensuring that any variations in the light source are included in both spectra, and are removed by normalization. This is often accomplished by placing a metal mesh upstream of the sample to that will allow the majority of the X-rays to pass through while absorbing a fraction. The current produced in the metal from the absorption of X-rays can be monitored which is proportional to the amount of incident X-rays. These metals have a smooth response of absorption with changing

illumination energy (with the exception of near the absorption edges). These well-known absorption characteristics allow them to be used over a large range of energies.

Since PEEM is a spectromicroscopy technique the I_0 can be recorded from a clean area of the substrate. This may only work if the sample can be made in such a way that there is an area of clean substrate in close proximity to the area of interest, and the absorption spectrum of the substrate has no spectral features in the desired energy range. This "internally" collected I_0 will not have an energy shift relative to the I, which can occur when scans are taken sequentially. This reference area can be created by removing a section of the sample to expose the silicon substrate, by removing a portion of the sample with a razor blade for example. This is the optimal scenario for normalization, as both the I and I_0 are obtained at the same time and place in the beamline.

While the best I_0 measurements are taken at the same time as the I, this may not be possible in all cases. The carbon absorption on optics will also occur on metal meshes used to monitor photocurrents, and a fresh coat of metal must be regularly deposited to keep the mesh surface clean. The I_0 may also not be able to be collected from a clean portion of the substrate, due to the small beam spot size, or the inability to produce a sample in such a way. This leaves the I_0 to be collected with a separate clean reference sample, measured either before or after the I spectrum is collected. This may be from a clean sample in the main chamber, such as a gold foil, or from a removable photodiode placed upstream from the main chamber for this specific purpose.

A major drawback to obtaining the I_0 at a separate time than the I is that the energy scale can change between scans. At different times, the energy scale of the monochromater may change by small amount. Movements of mechanical components of the beamline, positions of optical elements, position of the electron beam in the storage ring of the synchrotron, and heat load on optical elements can all have an effect on the energy scale[43]. These differences between the measured and reference spectra can lead to normalization artefacts and must be accounted for during normalization.

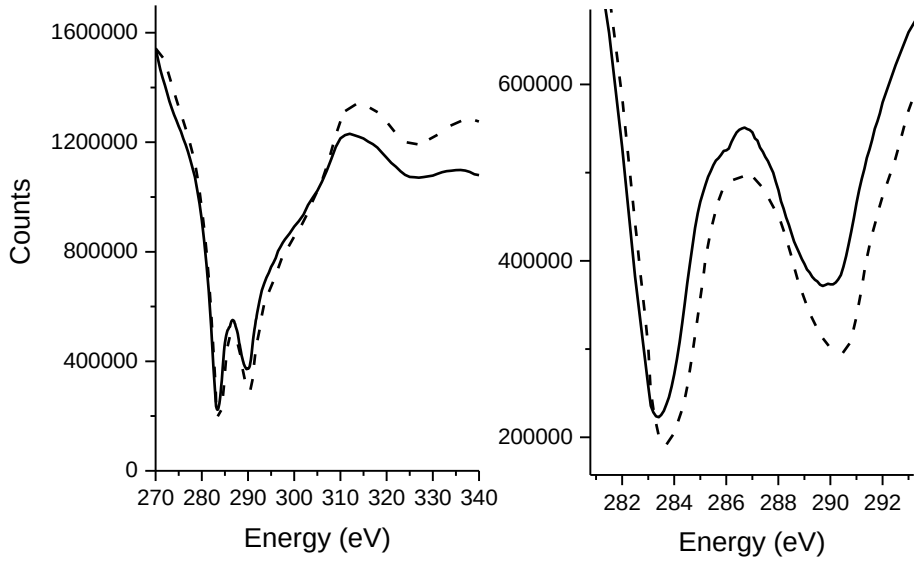

Figure 3-5: Two photo diode scans obtained on different days. The left spectrum shows the entire energy range while the right spectra show the detail of the carbon dip region.

Figure 3-5 shows two photodiode spectra that were obtained on different days. Differences between the two overlaid spectra are clearly visible, in particular in the details of the carbon dip region where there is a visible shift in the energy where the dips are located. A change in the structure of the high energy region is also visible in the spectra. If these factors are not properly corrected, significant artefacts will be present in the normalized spectrum. Artefacts are errors the represented data that have been introduced by the technique. Normalization artefacts may be introduced to the spectrum as a result of carbon contamination of the I_0 spectrum, dark noise, offset currents, or photon energy measurement due to monochromator fluctuations. These factors must be addressed in order to obtain quality spectra.

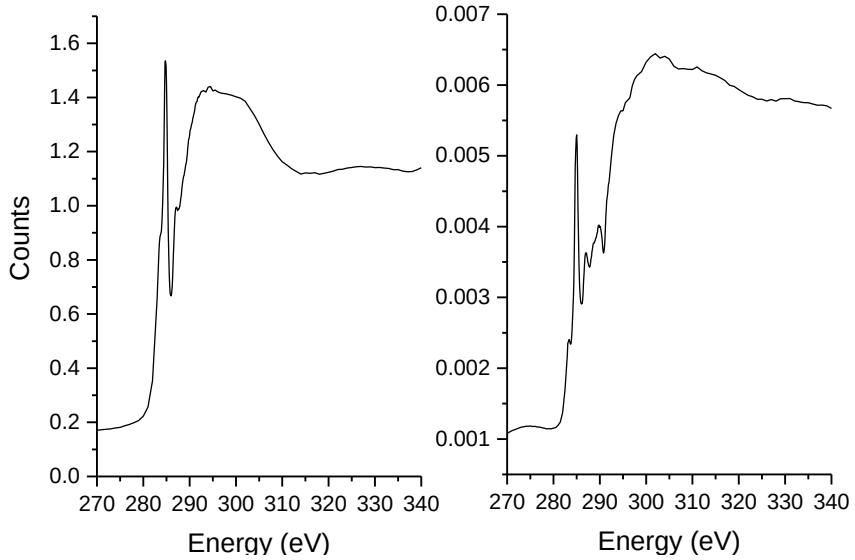

Figure 3-6: Normalized spectra using a simultaneously obtained I_0 (left) and a separately obtained photodiode I_0 (right).

Figure 3-6 shows two spectra that were normalized by a simultaneously collected I_0 collected from a clean area of the sample substrate (left) and from a previously obtained photodiode I_0 (right). The I_0 spectra used for normalization are the same ones shown in Figure 3-5. The spectrum normalized with the photodiode I_0 (right) has several peaks not seen in the spectrum normalized with the simultaneously collected I_0 (left), as well as a large reduction in the peak at 285 eV. There are also noticeable changes to the extended structure of the spectrum. These peaks are not features of the spectrum, but are artefacts introduced from improper normalization. With proper data handling, the presence of normalization artefacts can be controlled and allow I_0 obtained from spectra obtained from different times to be used for normalization.

3.2.2 Normalization Solutions and Procedures

The basic normalization procedure requires the sample spectrum to be divided by the reference spectrum (I/I_0). In reality it is not always as simple as this and there are several steps that need to be taken before this is able to be completed. In this section, a normalization example will be given with a polystyrene sample where spin casting was used to deposit the sample on a silicon substrate. Figure 3-7

shows the polystyrene sample and the corresponding spectra. The silicon substrate (bright area) has been exposed by scratching the polystyrene away with a razor blade to reveal the clean substrate. This produces an internal normalization, where the I and I_0 spectra are recorded simultaneously on the same surface.

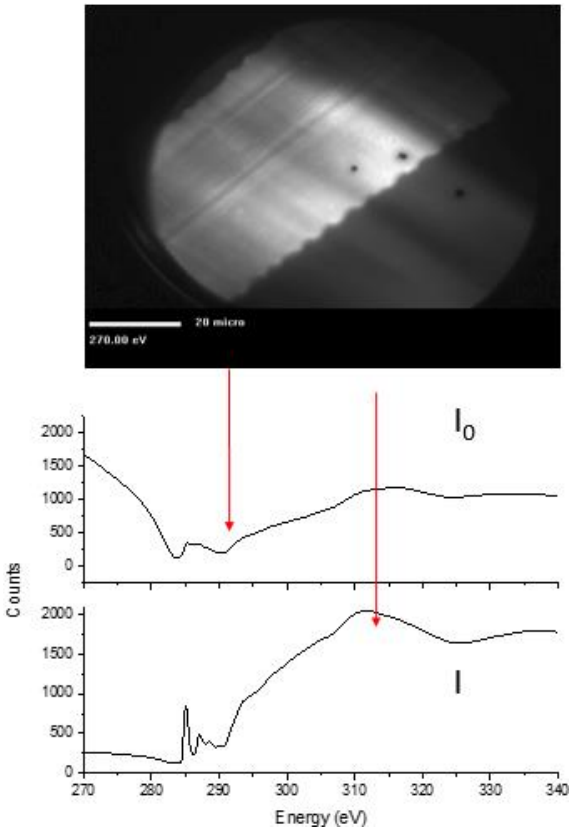

Figure 3-7: Image of 80 nm thick polystyrene film on silicon (top, 50 µm FOV) and the corresponding spectra from each area (bottom). The lower I spectrum is taken from a polystyrene area, while the upper I_0 spectrum is from the exposed silicon substrate.

The first step in the normalization procedure is to remove the dark noise from both the I and I_0 spectrum. The I and I_0 measurements do not only contain the desired information, but also contain dark noise. To obtain a measurement of the dark noise, the beamline shutter is closed for the first data points of each measurement in order to measure the dark noise of the spectrum. This dark noise will be removed from the spectra as a constant.

Figure 3-8 shows two spectra where the dark noise has not been removed (left) and where it has been removed. The two spectra are identical except for the beginning of the spectrum where there is no signal. The whole spectrum on the right has been shifted downwards to ensure that the beginning of the spectrum where there is no signal is at a value of 0. Dark noise is removed in the same manner for the I_0 spectra. Removing the dark noise from both the I and I_0 spectra ensures that artefacts are not introduced from the dark noise during normalization. The normalized spectra are truncated to remove the portion with zero signal.

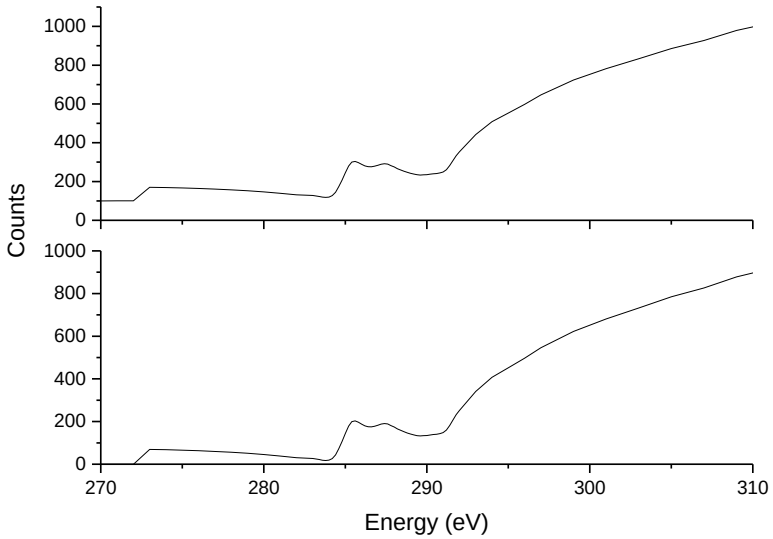

Figure 3-8: Measured spectrum (I) where the shutter is closed at the beginning to measure the dark noise. The left spectrum does not have the dark noise removed, while the right spectrum does. The value for the dark noise is 100.25

The dark noise is a background signal that can arise from multiple sources, such as electronic noise from the CCD camera, interference from electronics, from the MCP, among others. The dark noise does not create significant difficulties in situations where the measurements have intensities march larger than the level of the dark noise. The dark noise is significant for this experiment however as the X-ray beam has fairly low intensity in the energy range near the carbon dip and significant artefacts will be introduced to the normalized spectrum if the dark noise is not removed from both the I and I_0 before normalization. The I and I_0 that is measured contains the dark noise, as shown in the equation below:

$$Measured\ I = I + dark\ noise \quad (3.2)$$

If the dark noise is not removed from the I and I_0, then the normalization equation becomes:

$$\frac{I}{I_0} = \frac{I + dark\ noise}{I_0 + dark\ noise} \quad (3.3)$$

If the I and the I_0 become small relative to the dark noise, then the normalized spectrum will become distorted. For normalization to be applied successfully, the dark needs to be removed and the spectrum normalized by the following equation:

$$\frac{I}{I_0} = \frac{Measured\ I - dark\ noise}{Measured\ I_0 - dark\ noise} \quad (3.4)$$

The upper spectrum in Figure 3-8 has a dark noise value of 100.25, while the counts at the minimum of the carbon dip at ~285 eV are 120.0, putting the signal from the sample at this energy to only 19.75 average counts. The dark noise is very large relative to the signal, so large artefacts will be present in the normalized spectrum. Figure 3-9(a) shows a normalized spectrum of polystyrene where the dark noise has not been removed before normalization. The spectrum has several artefacts because of this including a peak before the main absorption edge, as well as erroneous peaks after the absorption edge. Figure 3-9(b) shows the normalized spectrum of the same polystyrene sample where the dark noise has been removed prior to normalization. While some artefacts still exist in the spectrum, notably a small shoulder peak in the pre-edge area denoted with an asterisk, the spectrum is much clearer.

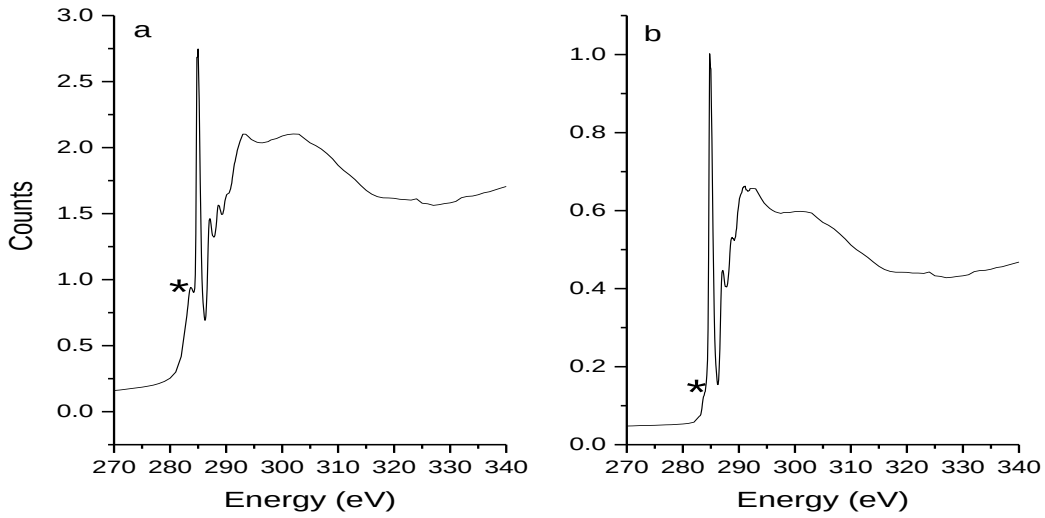

Figure 3-9: (a) A normalized spectrum of 80 nm polystyrene on silicon substrate where the I_0 has been taken from a clean area of the bare silicon substrate. Normalization artefacts are present both before (indicated with *) and after the peak at the carbon 1s absorption edge. (b) The normalized spectrum after the dark noise has been removed.

The surface of the sample is uniformly covered for alkane sample, and unlike the polystyrene example shown previously, the sample preparation method for alkanes does not give the opportunity to remove a portion of the sample to expose the substrate. This means that the I_0 spectra are not able to be obtained simultaneous to the spectra for the samples. This requires that the data from the I and I_0 spectra be handled properly in order to be normalized without introducing artefact to the spectrum. For separately recorded reference spectra, it is important to account for any energy shifts that might have occurred, as described previously. If there is a shift in energy, the I_0 is adjusted by shifting the energy scale of the entire spectrum to align with features present in both the I_0 and the I spectrum. For the raw data, the sharp drop in the intensity of the X-rays before the carbon 1s absorption edge is aligned with both spectra before normalization.

3.3 PEEM Results

There are several challenges relating to the X-ray absorption study of *n*-alkanes due to sensitivity to radiation. In addition, other challenges needed to be overcome in order to collect orientation specific

spectra of alkane domains include charging effects observed on the sample, as well as beam motion and structure observed in the beam. These negatively affect the quality of the spectra that are obtained, and strategies need to be formulated to ensure that useful data can be extracted from the spectra. The following section details these challenges and the steps taken to address them.

3.3.1 Radiation Damage and Reduction Strategies

A major obstacle to the study of *n*-alkanes using NEXAFS is degradation of the samples due to radiation. Alkanes have rich radiation chemistry due to efficient energy transfer. Products of radiation induced energy transfer in alkanes include H_2 gas, alkyl radical production, and cross linking of molecular chains[44]. In order to ensure the sample is not significantly damaged and these products are not generated in high quantity, care must be taken to keep the radiation dose on the sample as low as possible. The effect of radiation on *n*-alkane films have been studied herein, and strategies have been applied to reduce the radiation damage incurred on the samples.

Figure 3-10 shows a composite optical microscope image of the damage caused to the sample by the X-ray beam. This particular sample is C36 produced in the laboratory thermal evaporator. The sample was studied with large doses of radiation at several areas of the sample. The width of the beam can be clearly seen over the area of the sample that has been irradiated. After one area is studied, the sample is translated so that a different area is illuminated by the beam. The X-ray beam strikes the sample at a glancing angle, spreading out in the horizontal direction leading to streaks of visible radiation damage. Greater details of the effects of radiation can be seen in Figure 3-11. A graphite flake is seen here that has been partially irradiated. Loss of the alkane's orientations can be clearly seen on the lower half of the flake that has been in the X-ray beam (circled areas). The upper region of the flake appears to still be of good quality however.

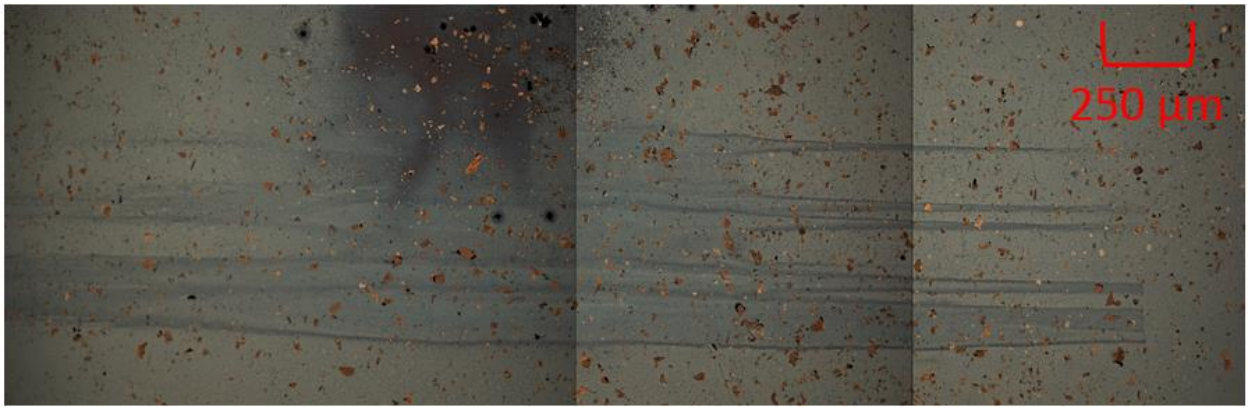

Figure 3-10: Composite optical microscope image (10X objective) of radiation damage on a C36 sample. Damage is small towards the ends of the beam

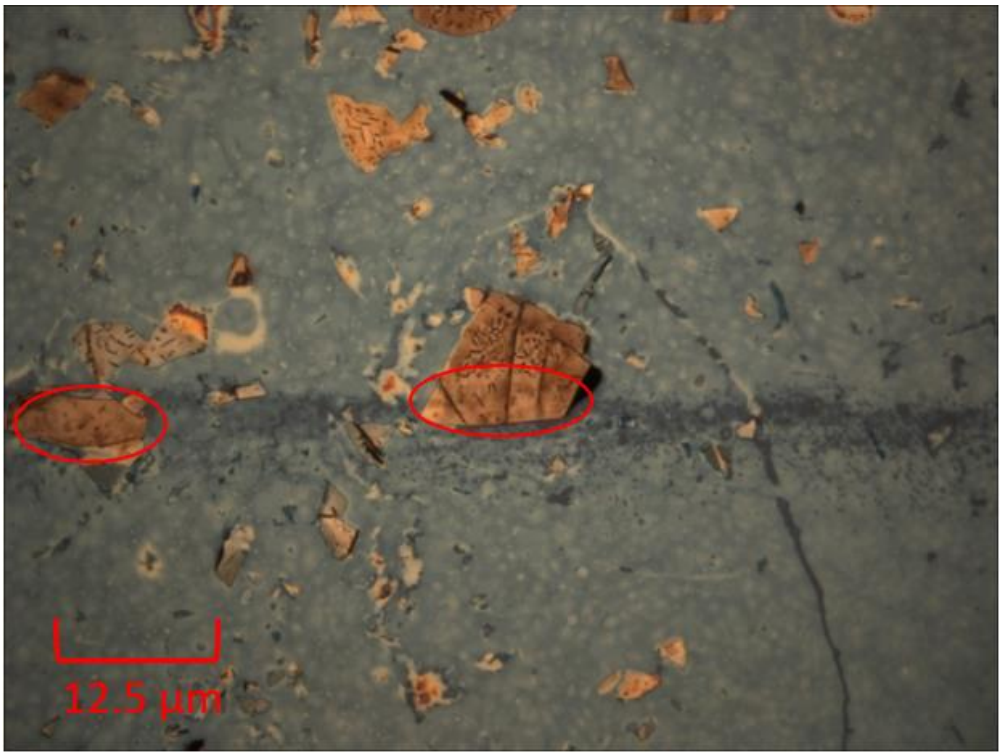

Figure 3-11: Optical microscope image (100X objective) of a graphite flake with C36 deposited after irradiation. Areas with radiation damage are circled.

Radiation damage is not only visible under optical microscopy, but can also be characterized by observing changes in the spectra. Figure 3-12 shows multiple spectra recorded with increasing time under the beam. As the time exposed to X-rays increases, the π* peak at 285 eV grows larger, while the σ* at 287 eV becomes smaller. This is indicative of crosslinking between carbon chains forming, increasing the

unsaturation in the sample, and therefore the π* peak. Loss of mass is also evident as the intensity of the extended spectrum lowers with each additional measurement. The mass loss is from H_2 formation as well as loss of carbon.

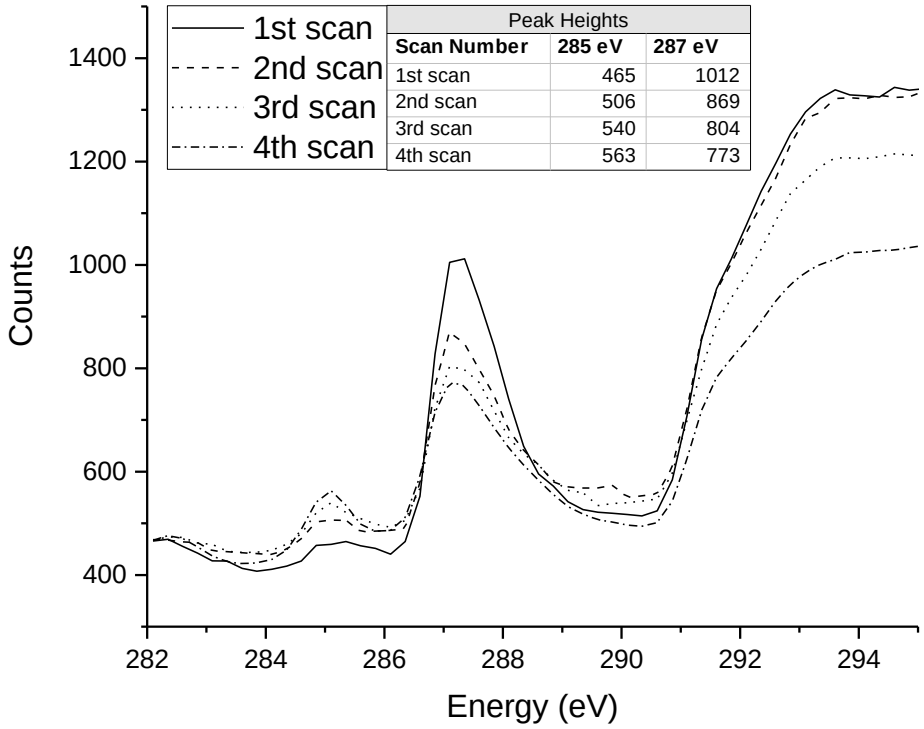

Figure 3-12: A spectral comparison of an area of alkane of a graphite flake. The σ* peak at 287 eV grows smaller, while the π* peak at 285 eV grows larger as the sample is damaged by radiation. Vertical polarization.

Different approaches have been investigated to minimize the exposure to excessive radiation that could damage the sample. To avoid radiation damage, unnecessary exposure to the beam is kept to a minimum by shuttering the beam while the energy is changed during a scan, lowering the dwell time when taking data points, and reducing the overall intensity of the light hitting the sample. As seen from Figure 3-11, areas of the sample that have not been irradiated remain in good condition, and the sample can be translated to a fresh area for successive measurements. Spectra are also taken near the edge of the beam. It can be seen from Figure 3-10 that the area near the edge of the beam cause far less damage that

the center. The intensity at the edges is approximately 60% less than at the center. When these factors are combined, the damage to the sample from the X-ray beam can be minimized, and data of suitable quality can be obtained, such as the first scan in Figure 3-12.

3.3.2 Beam Motion

Another difficulty encountered was change in the beam position on the sample with changing energy. The monochromator and optical components of the beamline and introduce structure to the beam, and care must be taken to ensure that this does not affect the spectra that are obtained. Figure 3-13 shows a graphite flake with C36 deposited at two different illumination energies of one eV difference. As the monochromator changes position, the light and darks streaks present in the beam also move across the surface of the sample.

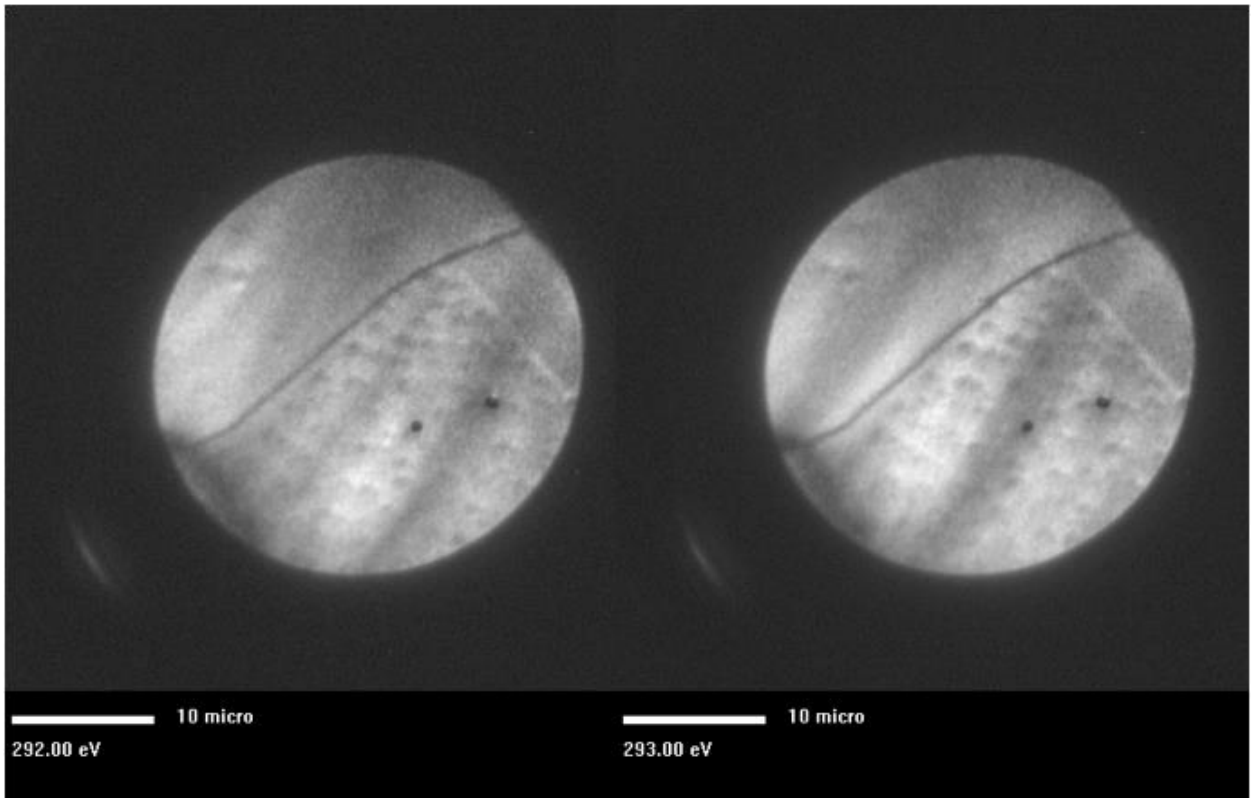

Figure 3-13: A sample of C36 on graphite/$Si0_2$ (50µm FOV). Note the streaks in the beam, and how they appear at different positions on the sample at only 1 eV difference.

The structure of the beam was found to be related to the slit settings of the beamline. When the slit openings are larger, the flux of the beamline increases, at the cost of reduced energy resolution. When the slit openings are small, the beam becomes dimmer while the energy resolution is increased. This is due to diffraction of the X-ray beam when the slit size is small. While low beam flux can hinder measurements of most samples, the reduction of the beam brightness as well as an increase in energy resolution are both advantageous to this experiment, so the slit sizes were reduced. After a certain point the dark and bright lines appear in the beam and make spectral measurements impossible when the beam position changes with the monochromator. The slit sizes were thus carefully optimized to reduce the beam flux while keeping the sample uniformly illuminated.

3.3.3 Charging

An additional problem encountered was charging of the poorly conductive sample. The charging effect causes positive charge to be built up on the sample surface, which will deflect electrons as they escape the sample (see section 1.2). This causes the sample to defocus; the image will appear blurred and larger than it was if there was no charging. Charging can also cause discharges from the sample when built up charge is released quickly. The sudden discharge of electrons can cause voltage interlocks to engage on the instrument, and can even damage the sensitive amplifier and detector of the PEEM. When there is a large amount of electrons in a dielectric material such as an insulator or vacuum, charge can build up in the material. This build up a charge will cause the electrons ejected from the sample to become deflected. These effects reduce the spatial resolution of the image. For these reasons, care must be taken to minimize the effects of charging when studying poorly conductive samples with PEEM in order to obtain accurate spectromicroscopy measurements.

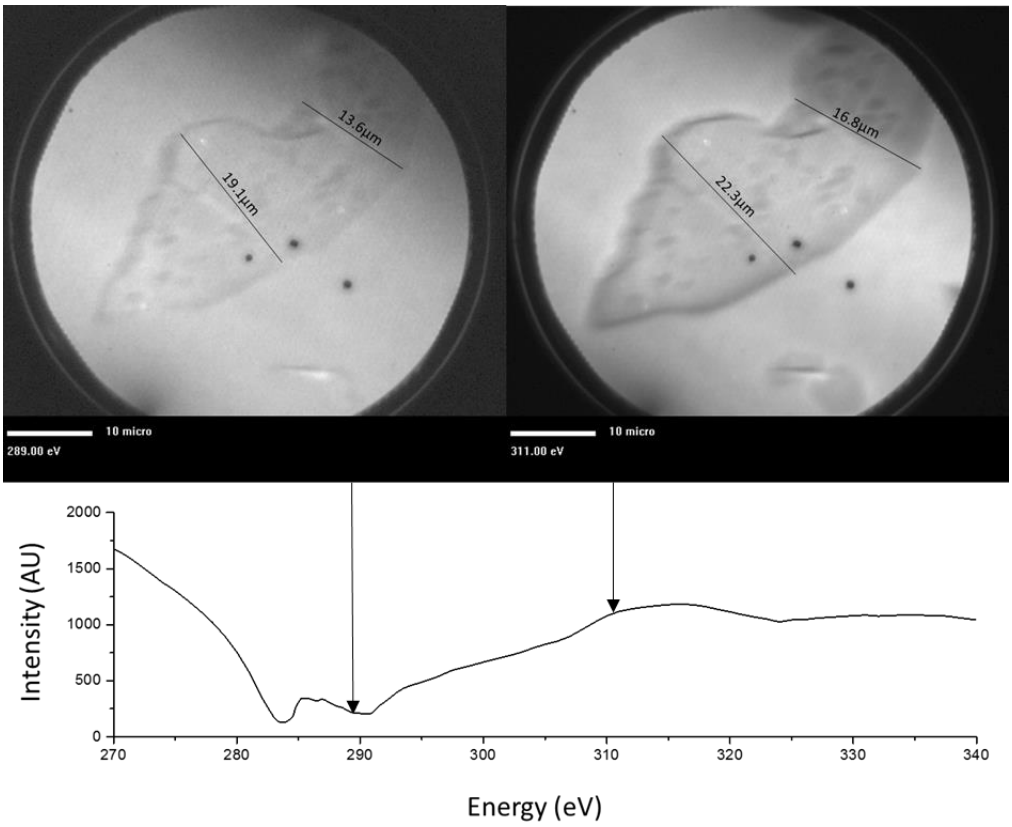

Figure 3-14: A sample of C36 on graphite/SiO_2 (50µm FOV). The graphite flake appears to be different sizes when X-rays at different energies are used to illuminate the sample. The X-ray energies that each image is measured at is indicated below.

If care is not taken when studying *n*-alkanes with PEEM the effects of charging can easily be seen. Figure 3-14 shows a C36 sample that is illuminated at two different X-ray energies. When the X-rays illuminating the sample are at 289 eV, the sample appeared to be smaller by about 17% when compared to the sample are 311 eV. The change in apparent size is caused by localized areas of positive charge build up, deflecting the trajectories of the emitted electrons and distorting the image.

As shown in Figure 3-14, the image taken at 289 eV (left) appears sharper and more focussed than the image taken at 311 eV (right). The lower amount of image distortion means that there is less charging present during illumination at 289 eV due to the lower flux of the beam when compared to illumination at 311 eV. The magnitude of the X-ray intensity is shown in the spectrum at the bottom of Figure 3-14. In order to minimize the charging, the flux of the beam is kept low. Keeping the intensity of

the beam low complements the radiation reduction strategy as well. While imaging of thing *n*-alkane films can be performed with a SiO_2 support if proper steps are taken, image quality will be reduced as a result.

3.3.4 Quality of Data

In order to keep the dosage of radiation to a minimum, the time the sample was in the X-ray beam had to be limited. This was accomplished by minimizing the time allotted for the software to measure data points (dwell time), as well as reducing the number of total data points. When combined with the reduced intensity of the beam, this creates noisy spectra. Care was taken to ensure that the method used provided spectra of sufficient quality, particularly over energy ranges where information about the orientation of carbon chains can be extracted.

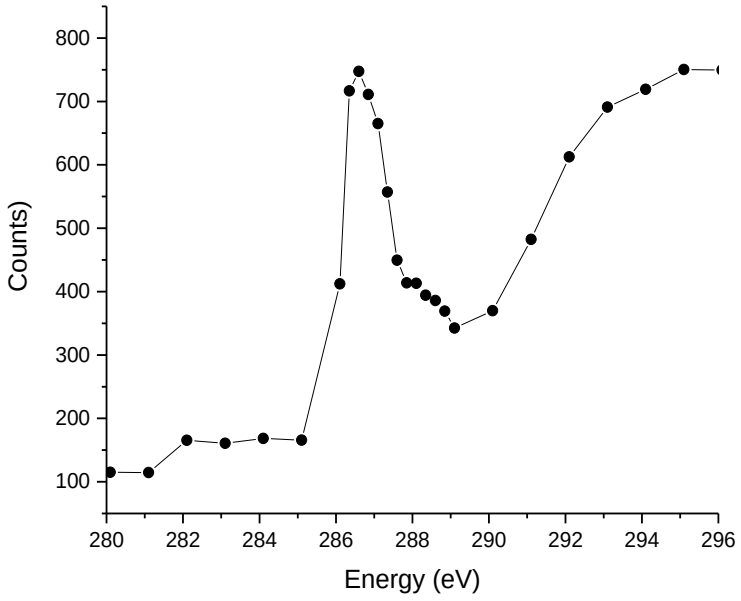

Figure 3-15: Raw spectrum from a C36 sample. The illuminating X-rays are vertically polarized.

Figure 3-15 shows a raw spectrum from a C36 sample. Before the sharp rise in absorption at 286 eV, data points are measured at 1 eV increments. Few data points are measured here because little important information is obtained from this region. From 286 eV to 289 eV data points are measured at

0.25 eV increments. The amount of data points measured here is increased as this is the region of the spectrum where the most details are. The increased number of data points are necessary to observe the 1s $\rightarrow\sigma^*_{C\text{-}H}$ transition at approximately 288 eV. Data points are taken at 1 eV increments from 289 eV to 296 eV. The reduced number of data points here minimizes the time the sample remains in the beam while still allowing the broad 1s $\rightarrow\sigma^*_{C\text{-}C}$ transition to be observed at 293 eV. The time the sample spends in the beam is also limited by having a dwell time for each data point of 50ms and averaging two measurements of each point. While limiting the number of measurements and the time taken for each data point leave the spectrum appearing noisy with straight sections between point as opposed to flowing curves, this reduction in time spent under the beam allows the relevant information about the heights of the 1s $\rightarrow\sigma^*_{C\text{-}H}$ and 1s $\rightarrow\sigma^*_{C\text{-}C}$ peaks to be extracted while avoiding radiation damage.

3.3.5 Spectra at Different Orientations

NEXAFS and PEEM can be used to determine the orientation of an ordered sample with spatial resolution (see sections 1.1.2 and 1.4.3). Spectra have been taken from sample where light and dark domains are present. These spectra are then compared with vertical and horizontal polarizations to determine the orientation of the alkane chains.

Figure 3-16 show a PEEM image of a typical sample created with the *ex situ* evaporator. Light and dark domains are seen and spectra are gathered from many areas to obtain a representation of the light and dark domains. Six-fold symmetry is not observed in these samples and patterns correspond to a pseudo-rectangular morphology where there is weak interaction between the alkane and the graphite substrate (see section 1.4.2, Figure 1-19 e and f). The poor quality of the image should also be noted, as the image appears fuzzy and out of focus. Difficulties focusing the PEEM can be attributed to small changes to the position and tilt of the sample, which are hard to correct without excess radiation exposure. While all possible care was taken to ensure the sample returned to the same position when returned to the PEEM main chamber, small changes to the tilt or position are unavoidable and could affect the focus of

the image. Some blurriness in the images may also be cause by the gain of the MCP which had to be increased to compensate for the lowered intensity of the X-ray beam.

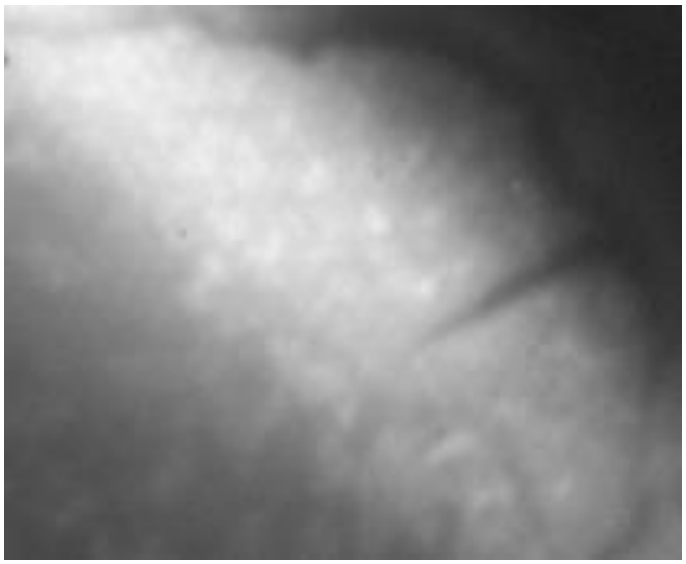

Figure 3-16: Graphite flake showing light and dark alkane areas (75 μm FOV). Image was obtained at an energy of 286.35 eV.

Figure 3-17 presents the NEXAFS spectra for the light and dark regions with vertical (a) and horizontal (b) polarizations. It can be seen from the spectra that there are no appreciable differences in the shape of the spectra over the energy range. The only difference between the spectra from the light and dark areas is a reduction in the number of counts of the dark spectrum evenly over the energy range. The dark areas are therefore assumed to be islands, as low areas of a PEEM sample appear brighter, whereas islands on the surface appear darker (see Figure 1-8a).

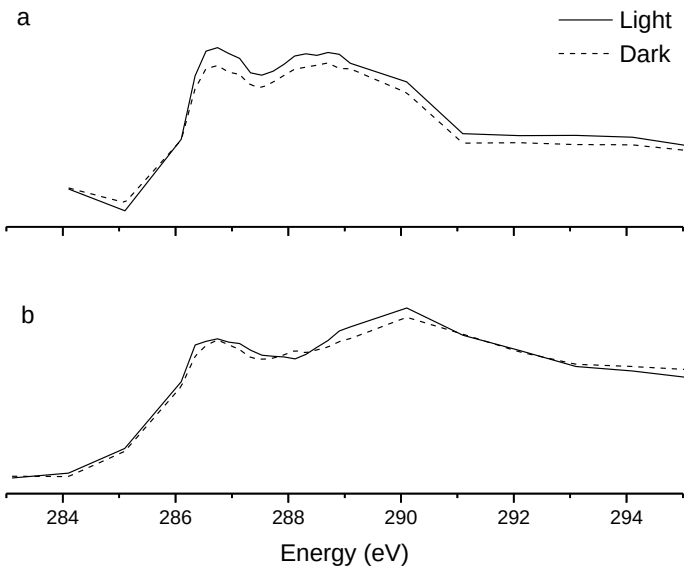

Figure 3-17: (a) Corresponding vertically polarized spectra of light and dark regions shown in Figure 3-16. (b) Horizontal polarized spectra of light and dark regions.

When comparing the spectra collected with different polarizations, a small inversion of the C-H and C-C absorption bands is observed. Figure 3-18 shows a maximum absorption in the C-H band with vertical polarization, whereas the maximum absorption occurs in the C-C band with horizontal polarization. This inversion of absorption maxima indicate the alkane chains are oriented normal to the graphite substrate.

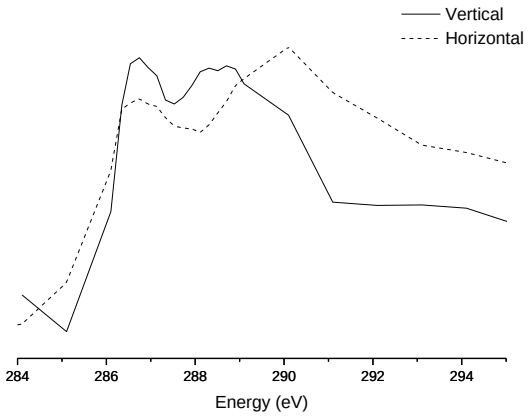

Figure 3-18: The vertical and horizontal polarized spectra for the light areas from Figure 3-17

Chapter 4 – Discussion

The focus of this thesis is on investigating the early to mid-stage growth of ordered *n*-alkane films on graphite. As previously demonstrated by Mitra Masnadi and Juxia Fu[7, 34, 39, 42, 45], the growth of *n*-alkane films on ordered substrates is dependent on the deposition conditions. Still it is not known how the growth mechanism changes as film thickness increases, and what factors drive these changes. The underlying mechanisms of film growth for these *n*-alkane thin films at early to mid-stages are difficult to investigate since the film must be observed at discrete intervals during film growth. A spatial and orientation sensitive technique is needed was to analyze thin *n*-alkane films as they grow.

To this end, PEEM and NEXAFS were used to study and characterize *n*-alkane thin films. These techniques provide an excellent way of obtaining structural and orientation information about the sample. By utilizing PEEM with polarized synchrotron light, chemical and orientation information was able to be obtained from the NEXAFS spectra collected from individual areas of the sample. While these are excellent techniques for studying thin *n*-alkane films, there are many unique challenges to the study *n*-alkanes, such as radiation sensitivity and vacuum compatibility. These problems need to be addressed before PEEM could be used to investigate the films. Chiefly among these issues was the ability to create samples where the film could be studied at different growth stages. To address this, a new *ex situ* evaporator was designed, assembled, and attached directly adjacent to the CaPeRS PEEM main chamber. The *ex situ* evaporator allowed successive depositions of *n*-alkanes to be used and thereby study the intermediate growth stages of these films.

The *ex* situ evaporator allowed *n*-alkane thin film samples to be prepared at the synchrotron beamline without exposing the sample to atmospheric conditions between evaporations. Preparing films on site was essential to preserve the film morphologies and was necessary to study changing growth

mechanisms as the thickness of the *n*-alkane thin films increases, through subsequent measurements on the same sample. The laboratory thermal evaporator was used to prepare films for initial film studies however, as this pre-existing evaporator setup allowed for a proven method of creating samples.

The *ex situ* evaporator was developed and demonstrated to be capable of creating ordered *n*-alkane films. The desired morphology with large ordered domains was not always obtained from the *ex situ* evaporator however. This was likely caused by poor temperature regulation of the sample heating stage. The *ex situ* evaporator also proved difficult to use, and the unreliable and time consuming process of sample preparation meant that the goal of successive depositions was never realized. Nevertheless, the *ex situ* evaporator allowed samples to be studied immediately after preparation, and could form the basis for future *n*-alkane studies with upgraded equipment.

There are many challenges associated using NEXAFS to study with *n*-alkanes due to the sensitivity of the films to X-ray and UV light. Therefore, an important step to this work was to develop a method that allowed spectra of *n*-alkanes to be gathered with minimal radiation damage where orientation information could still be extracted. The first issued to be address was normalization of NEXAFS data from C 1s spectra of *n*-alkanes. The synchrotron beamline used for PEEM has a large variation in X-ray intensity over the C 1s energy range due to adventitious carbon buildup on optical elements. Viewing the substrate before sample preparation allowed a I_0 spectrum to be collected, and the positions of the carbon dips were carefully monitored in both the I and I_0 spectra to adjust for any energy shifts caused by monochromator position fluctuations. The dark noise levels of the I and I_0 spectra were also carefully removed in order to avoid introducing normalization artefacts to the normalized spectrum. By taking these precautions, spectra could be acceptably normalized, even with the large carbon dips from the beamline.

Due to the sensitivity of *n*-alkanes to high energy radiation, steps were taken to minimize the amount of time samples spent under the X-ray beam, as well as limiting the overall intensity of the X-

rays, in order reduce the amount of radiation damage the samples exhibited. Through monitoring the π* peak at 285 eV, it was determined that this low intensity methodology was sufficient to prevent major damage to the samples. The large area of the samples also meant that an undamaged area was available for successive measurements.

During initial studies of *n*-alkane films created with the laboratory thermal evaporator, issues were encountered with charging due to the insulating 90 nm thick SiO_2 layer on top of the silicon support for the graphite/graphene substrate. It was determined experimentally however that charging did not cause samples to be unsuitable for PEEM when low intensity X-rays were used. This strategy of minimizing charging by limiting the intensity of the X-ray beam paired well with the method used for controlling radiation damage.

As a consequence of the strategies to reduce radiation damage and charging, the quality of the spectra that were collected was not as good as for a sample that is not prone to radiation damage or charging, since there needed to be less data points and a shorter dwell time at each photon energy interval. For example, compare the spectra from Figure 3-18 to the spectrum of a polystyrene film in Figure 4-1[35]. This relatively thick polystyrene film is much more robust than the *n*-alkane films, and as a consequence, spectra can be gathered with more data points and a longer dwell time. The peaks in Figure 4-1 sharp and well defined, while the peaks in the spectra of Figure 3-18 are broad and noisy. Even though the *n*-alkane spectra are of poor quality, the relevant peaks are able to be distinguished from the spectra, allowing sample orientation to be determined.

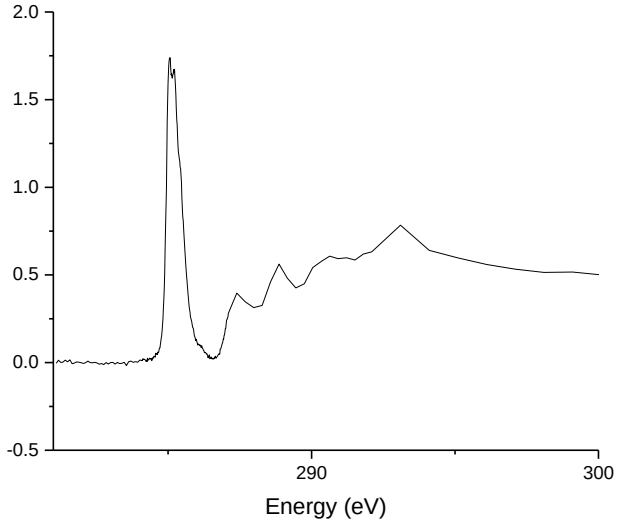

Figure 4-1: A spectrum of a 1000 Å thick polystyrene film. Data courtesy of Stephen Urquhart, originally published in Urquhart *et al.*[35].

This work has demonstrated that PEEM and NEXAFS have the potential to be powerful techniques for the observation of thin film growth. However, there remain several difficulties that need to be addressed before this technique can be successfully applied to the study of the early to mid-stage growth mechanisms of thin alkane films. Due to the difficulties with sample temperature stability discussed below, it was found that the pseudo-rectangular morphologies of C36 were the easiest to reliably produce, and were therefore the ones studied for the majority of the project. While the pseudo-rectangular morphology was easy to reproduce, morphologies with large bars and six-fold symmetry (see section 1.4.2, Figure 1-19) were more difficult to create with the *ex situ* evaporator and were not well reproduced. The likely cause of this is temperature fluctuations of the substrate during sample preparation.

The main difficulties encountered during sample preparation that were in regards to the heating of the substrate surface. As the sample being studied was in vacuum, there was no way for the sample to cool by convection, and the only means of sample cooling was radiatively. At the moderate temperatures used for sample preparation, small variations to the current of the heating filament would result in large

changes to the sample temperature that would take significant time to stabilize. In addition, there may have been an energy transfer to the substrate from the arrival of the *n*-alkane, or there could be a temperature change due to enthalpy of deposition. These temperature changes could have a large impact on the observed morphologies of the films produced. While all possible care was employed to minimize the temperature variations during deposition, it was nevertheless difficult to precisely control the sample temperature.

In order to realize the full potential of this technique, upgrades need to be made to the experimental equipment to address the above mentioned challenges. To concentrate on sample preparation challenges, a heat sink or active cooling could be installed in the sample holder or heating stage. This would create more conductive cooling of the sample and cause the sample temperature to be more stable during alkane deposition. As for the instrument itself, monochromator upgrades would help to reduce beam motion and uniformity. These solutions are not trivial to implement however, and are beyond the scope of this project.

There is currently a proposal to upgrade the CaPeRS X-PEEM[46] which would address some of the issues mentioned above. In particular, the proposal suggests a realignment of the microscope to provide brighter and more unified illumination. This would help to alleviate some of the focusing and tilt alignment issues discussed in section 2. The proposal also suggests intensity filters to be available for use with radiation sensitive samples, as well as an improved photon shutter. The proposal also contains provisions to improve simultaneous I_0 collection, reduce "stripes" in the beam spot, and more reliable sample manipulation tools. These improvements would allow easier and more successful observation of thin *n*-alkane films.

Chapter 5 - Conclusions

An *ex situ* evaporator was developed for use on the CaPeRS PEEM endstation of the SM beamline at the CLS. Pseudo-rectangular morphologies of C36 were grown in the *ex situ* evaporator, and the orientation of their carbon chains was determined using linear polarized NEXAFS spectroscopy. The analysis of the carbon 1s NEXAFS spectra show that the alkane chains are lying parallel to the substrate surface in this morphology. The work outlined here affirms previous observations that the orientations of alkane chains of pseudo-rectangular morphologies are lying parallel to the surface of the substrate. The quality of the data that was able to be gathered was, however, inadequate to examine the changes in growth mechanism (sections 1.4.2 and 1.4.4) believed to occur in early to mid-stage growth of *n*-alkane films.

In addition to the difficulties with the sample, challenges were also encountered with the microscope and beamline. Beam motion across the sample that occurred when the monochromator changed positions meant that spectra could not be extracted from singular domains. The beam did also not uniformly illuminate the sample, but caused streaks of light across the surface, compounding the problems caused by the beam motion.

There are several modifications and upgrades that could be made to the evaporator and microscope that could alleviate some difficulties associated with this project. For example, a heat sink could be integrated to the sample holder to promote even heating during sample preparation, or temperature stability could also be obtained with a liquid cooling system such as the one used in the laboratory thermal evaporator. In addition, monochromator upgrades and beamline improvements could be made to address the instability of the X-ray beam. Implementing these suggestions is not a trivial task however, and the time required alone puts these procedures outside the scope of this project. Nevertheless, this

work demonstrates the feasibility of using PEEM to study the growth of *n*-alkanes, and additional work in the future may be able to provide a better understanding of the growth mechanisms *n*-alkane films.

References

1. Strickland, W. P., Optical Thin Film Technology-Past, Present, Future. *Proceedings of SPIE - The International Society for Optical Engineering* **1990,** *1323* (Optical Thin Films 3), 2-7.
2. Cooper, A. J.; Antrazi, S.; Knieriem, K., Advantages and Advancements in Biased Target Deposition for Optical Thin Films. *Annual Technical Conference Proceedings - Society of Vacuum Coaters* **2011,** *54th*, 295-298.
3. Ranieri, M. G. A.; Cilense, M.; Aguiar, E. C.; Silva, C. C.; Simoes, A. Z.; Longo, E., Electrical Behavior of Chemically Grown Lanthanum Ferrite Thin Films. *Ceramics International* **2016,** *42*, 2234-2240.
4. Gilbert, E. P.; White, J. W.; Senden, T. J., Evidence for Perpendicular n-alkane Orientation at the Liquid/Graphite Interface. *Chemical Physics Letters* **1994,** *227* (4–5), 443-446.
5. Rabe, J. P.; Buchholz, S., Commensurability and Mobility in Two-Dimensional Molecular Patterns on Graphite. *Science* **1991,** *253* (5018), 424-427.
6. McGonigal, G. C.; Bernhardt, R. H.; Thomson, D. J., Imaging Alkane Layers at the Liquid/Graphite Interface with the Scanning Tunneling Microscope. *Applied Physics Letters* **1990,** *57* (1), 28-30.
7. Fu, J.; Urquhart, S. G., Linear Dichroism in the X-ray Absorption Spectra of Linear n-Alkanes. *Journal of Physical Chemistry A* **2005,** *109* (51), 11724-11732.
8. Stohr, J., *NEXAFS Spectroscopy*. 1st ed.; Springer-Verlag: Heidelberg, **1992**; Vol. 25, p 403.
9. Henke, B. L.; Gullikson, E. M.; Davis, J. C., Interactions: Photoabsorption, Scattering, Transmission, and Reflection at E=50-30000 eV, Z=1-92. *Atomic Data and Nuclear Data Tables* **1993,** *54* (2).
10. Hahner, G., Near Edge X-ray Absorption Fine Structure Spectroscopy as a Tool to Probe Electronic and Structural Properties of Thin Organic Films and Liquids. *Chemical Society Reviews* **2006,** *35* (12), 1244-1255.
11. Krause, M. O., Atomic Radiative and Radiationless Yields for K and L Shells. *Journal of Physical and Chemical Reference Data* **1979,** *8* (2), 307-327.
12. Cooney, R. R.; Urquhart, S. G., Chemical Trends in the Near-Edge X-ray Absorption Fine Structure of Monosubstituted and Para-Bisubstituted Benzenes. *Journal of Physical Chemistry B* **2004,** *108* (47), 18185-18191.
13. Wormer, P. Electromagnetic Wave. https://commons.wikimedia.org/wiki/File:Electromagnetic_wave.png.
14. Cossy-Favre, A.; Díaz, J.; Liu, Y.; Brown, H. R.; Samant, M. G.; Stöhr, J.; Hanna, A. J.; Anders, S.; Russell, T. P., X-PEEM Study on Surface Orientation of Stylized and Rubbed Polyimides. *Macromolecules* **1998,** *31* (15), 4957-4962.
15. Thome, J.; Himmelhaus, M.; Zharnikov, M.; Grunze, M., Increased Lateral Density in Alkanethiolate Films on Gold by Mercury Adsorption. *Langmuir* **1998,** *14* (26), 7435-7449.
16. Tsuruma, Y.; Al-Mahboob, A.; Ikeda, S.; Sadowski, J. T.; Yoshikawa, G.; Fujikawa, Y.; Sakurai, T.; Saiki, K., Real-Time Observation and Control of Pentacene Film Growth on an Artificially Structured Substrate. *Advanced Matererials* **2009,** *21* (48), 4996-5000.
17. Gilbert, B.; Andres, R.; Perfetti, P.; Margaritondo, G.; Rempfer, G.; De Stasio, G., Charging Phenomena in PEEM Imaging and Spectroscopy. *Ultramicroscopy* **2000,** *83* (1–2), 129-139.
18. *CRC Handbook of Chemistry and Physics*. 97th ed.; CRC Press/Taylor & Francis: Boca Raton, FL, **2016**.

19. Stohr, J.; Anders, S., X-ray Spectromicroscopy of Complex Materials and Surfaces. *IBM Journal of Research and Development* **2000,** *44* (4), 535-551.
20. Siegrist, K.; Williams, E. D.; Ballarotto, V. W., Characterizing Topography-Induced Contrast in Photoelectron Emission Microscopy. *Journal of Vacuum Science and Technology A* **2003,** *21* (4), 1098-1102.
21. Shinotsuka, H.; Tanuma, S.; Powell, C. J.; Penn, D. R., Calculations of Electron Inelastic Mean Free Paths. X. Data for 41 Elemental Solids Over the 50 eV to 200 keV Range with the Relativistic Full Penn Algorithm. *Surface and Interface Analysis* **2015,** *47* (9), 871-888.
22. Frazer, B. H.; Gilbert, B.; Sonderegger, B. R.; De Stasio, G., The Probing Depth of Total Electron Yield in the Sub-keV Range: TEY-XAS and X-PEEM. *Surface Science* **2003,** *537* (1-3), 161-167.
23. Genzer, J.; Sivaniah, E.; Kramer, E. J.; Wang, J.; Koerner, H.; Xiang, M.; Char, K.; Ober, C. K.; DeKoven, B. M.; Bubeck, R. A.; Chaudhury, M. K.; Sambasivan, S.; Fischer, D. A., The Orientation of Semifluorinated Alkanes Attached to Polymers at the Surface of Polymer Films. *Macromolecules* **2000,** *33* (5), 1882-1887.
24. Hamamatsu Photonics, K. K., MCP and MCP Assembly. **2016**.
25. Veser, G.; Esch, F.; Imbihl, R., Regular and Irregular Spatial Patterns in the Catalytic Reduction of Nitric Oxide with Ammonia on Platinum (100). *Catalysis Letters* **1992,** *13* (4), 371-82.
26. Herman, M. A.; Richter, W.; Sitter, H., *Epitaxy. Physical Principles and Technical Implementation by M. A. Herman, W. Richter, and H. Sitter*. 1st ed.; Oldenbourg Wissenschaftsverlag GmbH: **2004**; Vol. 219, p 768-769.
27. Venables, J. A.; Spiller, G. D. T.; Hanbuecken, M., Nucleation and Growth of Thin Films. *Reports on Progress in Physics* **1984,** *47* (4), 399-459.
28. Hooks, D. E.; Fritz, T.; Ward, M. D., Epitaxy and Molecular Organization on Solid Substrates. *Advanced Materials* **2001,** *13* (4), 227-241.
29. Masnadi, M.; Urquhart, S. G., Indirect Molecular Epitaxy: Deposition of n-Alkane Thin Films on Au Coated NaCl(001) and HOPG(0001) Surfaces. *Langmuir* **2013,** *29* (21), 6302-6307.
30. Kubono, A.; Akiyama, R., Classical Nucleation Theory Applied to Molecular Orientations in Vapor-Deposited Organic Thin Films. *Journal of Applied Physics* **2005,** *98* (9), 093502/1-093502/6.
31. Leunissen, M. E.; Graswinckel, W. S.; van Enckevort, W. J. P.; Vlieg, E., Epitaxial Nucleation and Growth of n-Alkane Crystals on Graphite (0001). *Crystal Growth and Design* **2004,** *4* (2), 361-367.
32. Kubono, A.; Akiyama, R., Orientational Mechanism for Long-Chain Organic Molecules During Physical Vapor Deposition. *Molecular Crystals and Liquid Crystals* **2002,** *378*, 167-183.
33. Tanaka, K.; Okui, N.; Sakai, T., Molecular Orientation Behavior of Paraffin Thin Films Made by Vapor Deposition. *Thin Solid Films* **1991,** *196* (1), 137-45.
34. Masnadi, M.; Urquhart, S. G., Effect of Substrate Temperature on the Epitaxial Growth of Oriented n-Alkane Thin Films on Graphite. *Langmuir* **2012,** *28* (34), 12493-12501.
35. Urquhart, S. G.; Ade, H.; Rafailovich, M.; Sokolov, J. S.; Zhang, Y., Chemical and Vibronic Effects in the High-Resolution Near-Edge X-ray Absorption Fine Structure Spectra of Polystyrene Isotopomers. *Chemical Physics Letters* **2000,** *322* (5), 412-418.
36. Stumm von Bordwehr, R., A History of X-ray Absorption Fine Structure. *Annals of Physics* **1989,** *14* (4), 377-466.
37. Urquhart, S. G.; Lanke, U. D.; Fu, J., Characterisation of Molecular Orientation in Organic Nanomaterials by X-ray Linear Dichroism Microscopy. *Intnational Journal of Nanotechnology* **2008,** *5* (9/10/11/12), 1138-1170.
38. Jakubith, S.; Rotermund, H. H.; Engel, W.; Von Oertzen, A.; Ertl, G., Spatiotemporal Concentration Patterns in a Surface Reaction: Propagating and Standing Waves, Rotating Spirals, and Turbulence. *Physical Review Letters* **1990,** *65* (24), 3013-16.

39. Masnadi, M. Kinetics and Thermodynamics of *n*-Alkane Thin Film Epitaxial Growth. University of Saskatchewan, Saskatoon Saskatchewan, **2013**.
40. Novoselov, K. S.; Geim, A. K.; Morozov, S. V.; Jiang, D.; Zhang, Y.; Dubonos, S. V.; Grigorieva, I. V.; Firsov, A. A., Electric Field Effect in Atomically Thin Carbon Films. *Science* **2004,** *306* (5696), 666-669.
41. Blake, P.; Hill, E. W.; Castro Neto, A. H.; Novoselov, K. S.; Jiang, D.; Yang, R.; Booth, T. J.; Geim, A. K., Making Graphene Visible. *Applied Physics Letters* **2007,** *91* (6), 063124.
42. Fu, J. Linear Dichroism in the NEXAFS Spectroscopy of n-alkane Thin Films. University of Saskatchewan, Saskatoon Saskatchewan, **2006**.
43. Schöll, A.; Zou, Y.; Schmidt, T.; Fink, R.; Umbach, E., Energy Calibration and Intensity Normalization in High-Resolution NEXAFS Spectroscopy. *Journal of Electron Spectroscopy and Related Phenomena* **2003,** *129* (1), 1-8.
44. Partridge, R. H., Excitation Energy Transfer in Alkanes. III. Radiation Chemistry of Alkane Polymers. *Journal of Chemical Physics* **1970,** *52* (5), 2501-10.
45. Fu, J.; Urquhart, S. G., Effect of Chain Length and Substrate Temperature on the Growth and Morphology of n-Alkane Thin Films. *Langmuir* **2007,** *23* (5), 2615-2622.
46. Urquhart, S. *Conceptual Design Report for the CaPeRS X-PEEM Upgrade*; **2014**.